Published in final edited form as:
J Comp Neurol. 2009 January 20; 512(3): 399–418. doi:10.1002/cne.21896.

Axospinous synaptic subtype-specific differences in structure, size, ionotropic receptor expression, and connectivity in apical dendritic regions of rat hippocampal CA1 pyramidal neurons

Daniel A. Nicholson[1,*] and **Yuri Geinisman**[1]
Dr. Oswald Steward
[1]Department of Cell and Molecular Biology, Northwestern University Feinberg School of Medicine, Chicago, Illinois 60611 U.S.A.

University of California-Irvine; Cellular Neurobiology and Neuronal Plasticity

Abstract

The morphology of axospinous synapses and their parent spines varies widely. Additionally, many of these synapses are contacted by multiple synapse boutons (MSBs) and show substantial variability in receptor expression. The two major axospinous synaptic subtypes are perforated and nonperforated, but there are several subcategories within these two classes. The present study used serial section electron microscopy to determine whether perforated and nonperforated synaptic subtypes differed with regard to their distribution, size, receptor expression, and connectivity to MSBs in three apical dendritic regions of rat hippocampal area CA1: the proximal and distal thirds of stratum radiatum, and stratum lacunosum-moleculare. All synaptic subtypes were present throughout the apical dendritic regions, but there were several subclass-specific differences. First, segmented, completely partitioned synapses changed in number, proportion, and AMPA receptor expression with distance from the soma beyond that found within other perforated synaptic subtypes. Second, atypically large nonperforated synapses showed NMDA receptor immunoreactivity identical to perforated synapses, levels of AMPA receptor expression intermediate to nonperforated and perforated synapses, and perforated synapse-like changes in structure with distance from the soma. Finally, MSB connectivity was highest in proximal stratum radiatum, but only for those MSBs comprised of nonperforated synapses. The immunogold data suggest that most MSBs would not generate simultaneous depolarizations in multiple neurons or spines, however, because the vast majority of MSBs are comprised of two synapses with abnormally low levels of receptor expression, or involve one synapse with a high level of receptor expression and another with only a low level.

Keywords

serial section analysis; immunogold electron microscopy; AMPA receptor; NMDA receptor; multiple synapse bouton; dendritic spine; postsynaptic density

The vast majority of excitatory synapses onto pyramidal neurons are on small, finger-like protrusions called dendritic spines (reviewed in Geinisman, 2000; Yuste and Bonhoeffer, 2001; Nimchinsky et al., 2002; Kasai et al., 2003; Hayashi and Majewska, 2005; Alvarez and Sabatini, 2007; Bourne and Harris, 2008). On the cytoplasmic face of each dendritic spine is the postsynaptic density (PSD), which is an electron-dense region containing

*Corresponding author: Dan Nicholson, Department of Cell and Molecular Biology, Northwestern University Feinberg School of Medicine, Chicago, Illinois 60611. E-mail: dnicholson@northwestern.edu

proteins involved in synaptic transmission, structural plasticity and stability, and intracellular signaling (reviewed in Kennedy, 2000; Scannevin and Huganir, 2000; Kim and Sheng, 2004; Funke et al., 2005; Kennedy et al., 2005; Sheng and Hoogenraad, 2007). The morphology of both the PSD and its parent spine varies widely, and to an extent this variability is thought to correlate with function (Nieto-Sampedro et al., 1982; Carlin and Siekevitz, 1983; Calverley and Jones, 1990; Geinisman et al., 1993; 2000; Jones and Harris, 1995; Lüscher et al., 2000; Kasai et al., 2003; Bourne and Harris, 2007, 2008).

Such heterogeneity in spine and synapse structure has been acknowledged previously (e.g., Gray, 1959; Westrum and Blackstad, 1962; Colonnier, 1968; Peters and Kaiserman-Abramof, 1969, 1970; Cohen and Siekevitz, 1978; Spacek and Hartmann, 1983; Dyson and Jones, 1984; Geinisman et al., 1986, 1987, 1993; Harris and Stevens, 1989). Generally, however, excitatory axospinous synapses can be classified into two major subtypes based on the configuration of their PSD: perforated and nonperforated. When viewed in serial sections, perforated synapses are those synapses that have at least one discontinuity or perforation in their PSD, whereas nonperforated synapses have continuous PSD profiles in all sections. Recently, studies using postembedding immunogold electron microscopy for synaptic receptors have provided detail regarding possible functional differences between these two synaptic subtypes (Desmond and Weinberg, 1998; Nusser et al., 1998; Takumi et al., 1999; Racca et al., 2000;Ganeshina et al., 2004a, 2004b; Nicholson et al., 2006).

The most parsimonious summary of the available data is that perforated synapses have a substantially higher number and density of immunogold particles for AMPA-type receptors (AMPARs); and a higher number, but lower density of immunogold particles for NMDA-type receptors (NMDARs). Because voltage signals (e.g., unitary potentials, dendritic spikes) are the principal means by which synapses can communicate with the action potential initiation zone in the axon (reviewed in Williams and Stuart, 2003; London and Häusser, 2005; Sjöström et al., 2008; Spruston, 2008), this account suggests that synaptic potentials originating at perforated synapses are the principal contributor to dendritic and somatic depolarization (Nicholson et al., 2006; Spruston, 2008). Nonperforated synapses are the most numerous, despite ~40% of them lacking AMPAR immunoreactivity. Rather than driving action potentials or dendritic spikes, however, many of these small, frequently "silent" nonperforated synapses may represent potential or nascent functional connections (Harris and Kater, 1994; Eichenbaum and Harris, 2000; Geinisman, 2000; Nimchinsky et al., 2002; Holtmaat et al., 2005; Knott et al., 2006; Nicholson et al., 2006; Toni et al., 2007).

Overlaid onto this general morphological distinction between perforated and nonperforated synapses is the observation that they are both structurally heterogeneous themselves. Specifically, the PSDs of perforated synapses can be fenestrated, horseshoe-shaped, or be comprised typically of two, or rarely 3 or 4, discrete PSD segments (Calverley and Jones, 1990; Geinisman, 1993; Jones and Harris, 1995; Muller, 1997; Nicholson et al., 2004). Nonperforated synapses, while always having a shape approximated by that of a continuous disc, can range in size by over an order of magnitude, with the largest ones having subcellular organelles that are found primarily in perforated synapses (Geinisman, 1993). These various synaptic subtypes have been interpreted to reflect static images of synapses cycling through structural alterations in response to changing levels of stimulation (Nieto-Sampedro et al., 1982; Carlin and Siekevitz, 1983; Geinisman, 1993).

Though this notion of synaptic cycling may be valid, many of the synaptic subtypes involved are also likely to exist stably at steady state because their distribution has functional consequences on dendritic integration (Nicholson et al., 2006; Spruston, 2008). For example, the number and level of AMPAR expression for perforated synapses depends on their distance from the soma (Nicholson et al., 2006). Such distance-dependent regulation

of number and receptor expression among perforated synapses helps counteract attenuation of synaptic potentials as they propagate through the cable-like apical dendrites of hippocampal CA1 pyramidal neurons (Magee and Cook, 2000; Smith et al., 2003; Nicholson et al., 2006; Spruston, 2008). Whether or not the different perforated synaptic subtypes are individually regulated with distance from the soma is unknown. One such synaptic subtype is the segmented, completely partitioned (SCP) synapse, which is characterized by multiple PSD plates, each of which is separated from the other by a spine partition that invaginates the presynaptic axon terminal (Geinisman, 1993). Our previous work has shown that SCP synapses have the highest number and density of immunogold particles for AMPARs, nearly twice that of other types of perforated synapses (Ganeshina et al., 2004b). If the distribution of excitatory synapses onto CA1 pyramidal neurons is regulated in part to compensate for the cable properties of dendrites, one might expect that SCP synapses, which according to their AMPAR expression may be the most efficacious of the different axospinous synaptic subtypes in the hippocampal CA1 region, change in number and strength as their dendritic position shifts progressively farther from the action potential initiation zone in the soma/axon.

Regardless of their PSD configuration, a sizeable subset of synapses shares a single presynaptic bouton (Sorra and Harris, 1993). Such multiple synapse boutons (MSBs) have been implicated in behavioral (Jones et al., 1997; Geinisman et al., 2001; Federmeier et al., 2002) and physiological/structural (Jones et al., 1999; Toni et al., 1999; 2007) plasticity, as well being affected by hormone levels (Woolley et al., 1996; Yankova et al., 2001). The prevailing notion regarding the function of MSBs is that they provide a mechanism by which a single presynaptic action potential can activate multiple postsynaptic neurons or spines (e.g., Harris, 1995; Toni et al., 1999). This idea, however, has never been addressed because it would involve live-cell imaging of the pre- and post-synaptic neurons, whole-cell somatic patch-clamp recordings from the presynaptic neuron to trigger action potentials, and dendritic whole-cell patch-clamp recordings from the postsynaptic neuron to estimate the strength of each of the synapses of a MSB. One approach that circumvents some of these challenges is to use postembedding immunogold electron microscopy of individual MSBs to determine the levels of AMPAR and NMDAR expression among their synapses. Though such an approach would provide only an estimate of the relative strength of each synapse at one point in time, inferences from such data could be made to more fully understand the function of MSBs.

Thus, the present study combined conventional and postembedding immunogold serial section electron microscopy to determine whether distance-dependent and synapse-specific differences exist in the fine structure and AMPAR and NMDAR expression of synapses involved in both single-synapse boutons and MSBs in three progressively distal regions of the apical dendrites of rat hippocampal CA1 pyramidal neurons: the proximal one-third of stratum radiatum (pSR), the distal one-third of stratum radiatum (dSR), and stratum lacunosum-moleculare (SLM).

MATERIALS AND METHODS

Animals

Six male, adult (6-months old), individually-housed F1 hybrid Fisher 344 × Brown Norway rats (Harlan, Indianopolis, IN) were used. The conventional and postembedding immunogold electron microscopic analyses each involved three rats. All experimental procedures were performed in accordance with NIH guidelines for the care and use of animals in research and were approved by Northwestern University's Animal Care and Use Committee.

Tissue preparation and analysis using conventional electron microscopy

Rats were deeply anesthetized with an intraperitoneal injection of a mixture of ketamine hydrochloride and xylazine (87 mg/kg and 13 mg/kg, respectively), and then perfused transcardially with 0.12M phosphate buffered saline (PBS; pH 7.4) for 1 minute, an aldehyde mixture of 1% paraformaldehyde and 1.25% glutaraldehyde in 0.12M PBS for 5 minutes, and the same fixative at twice the concentration for 10 minutes (Electron Microscopy Sciences, Fort Washington, PA). The dorsal hippocampus was dissected free and cut, perpendicular to its long axis, into 0.8 mm-thick slabs at systematic random intervals (Geinisman et al., 1996; Geinisman et al., 2000; 2004; Nicholson et al., 2006). These slabs were then treated with OsO_4, dehydrated in escalating concentrations of ethanol and propylene oxide, and flat embedded in Araldite (Electron Microscopy Sciences, Fort Washington, PA).

After measuring the thickness of hippocampal slabs with an inverted microscope and an oil-immersion lens, they were mounted and used to obtain 2 μm-thick histological sections, which were stained with azure II/methylene blue. Such sections were used for estimations of the volume of stratum radiatum (SR) and SLM, and to determine the sampling fields using systematic random sampling. Using a projection microscope (Ken-A-Vision, Raytown, MO), outlines of the sectional profiles of SR and SLM were drawn, and their areas were estimated using point-counting. Total volume was calculated as the product of their summed profile areas and the thickness of the tissue slabs. The volumes of pSR and dSR were each equal to one-third of the total SR volume (Nicholson et al., 2006).

Five slabs from each rat were chosen in a systematic random manner and each was used to obtain 27-35 serial sections, which were counterstained with 5% aqueous uranyl acetate and Reynold's lead citrate. Each section spanned the entire extent of the apical dendritic region of CA1 pyramidal neurons, from the pyramidal cell layer to the hippocampal fissure. The borders of pSR, dSR, and SLM were determined from the histological sections. Using the field delineator of the electron microscope (JEOL 100CX, JEOL Ltd. Tokyo, Japan), sampling fields from each of these regions were chosen in a systematic random manner. Electron micrographs (final magnification of 21,900×, as determined from using a grating replica from Electron Microscopy Sciences, Fort Washington, PA after each grid was photographed) of the systematic randomly determined sampling field were then obtained from each apical dendritic region on the same set of serial sections.

Synaptic numerical density was estimated using the physical disector method (20 disectors were used for each dendritic region from each slab). The total number of synapses was determined as the product of the volume of the dendritic region (in μm^3) and average synaptic numerical density (in synapses/μm^3) for each rat. Disector volume was estimated as the product of section thickness (0.075 mm using Small's method of minimal folds) and the area of the unbiased counting frame (72 μm^2) to be 5.4 μm^3. SCP ratio for each rat was calculated from the total number estimates as the number of SCP synapses divided by the number of all perforated synapses (including SCP synapses).

MSBs were quantified in each series as described previously (Geinisman et al., 2001). Briefly, 15 consecutive sections were selected with a random start from section 5, 6, or 7. These 15 serial sections were then used to estimate the numerical density of MSBs and their subtypes using the physical disector method. Choosing only a subset of sections for quantifying MSB number was necessary as it allowed us to follow boutons in their entirety for unequivocal identification of a bouton as nonsynaptic, monosynaptic, or multisynaptic. The numerical density of MSBs was then multiplied by the volume of the appropriate dendritic region to obtain estimates of their total number.

We constrained our morphological measurements to only those synapses whose spines could be traced back to their parent dendrites (Tables 1-3). Using ImageJ (Rasband, W.S.,ImageJ, U. S. National Institutes of Health, Bethesda, Maryland, USA, http://rsb.info.nih.gov/ij/, 1997-2007), a digitizing tablet (Wacom, Saitama, Japan), and the electron micrographs, we measured the total length and area of these synapses and spines, respectively. PSD area was estimated as the product of the total PSD length measured from all sections in which its profile was present and section thickness. Spine volume was calculated as the product of the total area of the spine sectional profiles and section thickness. In most cases, we were also able to measure other morphological features of the spines (Tables 1-3), but the functions of these parameters are not well-understood so they were not analyzed statistically. 3-dimensional reconstructions were made using Reconstruct (Fiala, 2005; freely available at http://synapse-web.org). Though there is a possibility that our measurements are biased toward shorter spines (due to our requirement that they be traceable back to their parent dendrite), the range of neck lengths in the present study is in agreement with measurements from other studies (e.g., Harris and Stevens, 1989).

Tissue preparation and analysis using postembedding immunogold electron microscopy

Expression of postsynaptic AMPARs and NMDARs was assessed as described previously (Ganeshina et al., 2004a, 2004b; Nicholson et al. 2006). Rats were deeply anesthetized with an intraperitoneal injection of a mixture of ketamine hydrochloride and xylazine (87 mg/kg and 13 mg/kg, respectively). Subsequently, they were perfused with a mixture of 4% paraformaldehyde and 0.5% glutaraldehyde (Electron Microscopy Sciences, Fort Washington, PA) in 0.12M PBS (pH 7.4). The sampling design specified above was used with the following modifications.

From each rat, the dorsal half of the hippocampus was cut into 0.3 mm-thick slabs, of which five were selected in a systematic random manner. These five slabs were then divided along their mediolateral extent into three slivers, each of 0.5 – 1.0 mm thickness. All of the slivers were then cryoprotected in escalating concentrations of glycerol and plunge-frozen in liquid propane at −184° C using a Leica EM CPC (Leica, Wien, Austria). Each sliver was then transferred to a Leica AFS freeze-substitution system, treated with 1.5% uranyl acetate (Electron Microscopy Sciences, Fort Washington, PA) in Fluka methanol (Sigma, St. Louis, MO) at −90° C, infiltrated with Lowicryl HM20 resin (Electron Microscopy Sciences, Fort Washington, PA) at gradually escalating temperatures, and polymerized with ultraviolet light at 0° C. One sliver from each slab was then used to prepare 17-33 serial ultrathin sections, which were mounted as a ribbon on gold-gilded nickel slot grids (Electron Microscopy Sciences, Fort Washington, PA). Minimal folds were rarely, if ever, present in the Lowicryl sections. Therefore, we approximated section thickness as 0.068 μm based on their silver interference color and the setting on the ultramicrotome (Ultracut 6, Leica, Wien, Austria).

Grids were etched briefly (~ 1 second) with ethoxide, treated with 0.1% sodium borohydride and 50 mM glycine in 5 mM Tris buffer (pH 7.4) containing 0.05% Triton X-100 (Sigma, St. Louis, MO) and 0.9% saline (TBST) for 10 minutes, rinsed in TBST, blocked with 10% normal goat serum (NGS; Electron Microscopy Sciences, Fort Washington, PA) in TBST for 30 minutes, and incubated overnight in a cocktail of primary antibodies to either AMPARs or NMDARs (Chemicon, Temecula, CA) dissolved in TBST with 1% NGS at 4° C. The primary antibody cocktail for AMPARs was comprised of GluR1 at 3.0 μg/ml, GluR2 at 1.5 μg/ml, GluR2/3 at 3.0 μg/ml, and GluR4 at 3.0 μg/ml. The primary antibody cocktail for NMDARs contained NR1 at 10.0 μg/ml and NR2A/B at 10.0 μg/ml. After thorough rinsing, grids were blocked with 1% NGS in TBST (pH 8.2) for 30 minutes, then incubated for 1 hour in a 1:20 dilution of secondary antibodies conjugated with 10-nm gold particles in the same solution at room temperature (British BioCell International, Cardiff,

UK), rinsed in TBST followed by ultrapure water, and allowed to air dry. Finally, sections were counterstained with 5% aqueous uranyl acetate and Reynold's lead citrate. Electron micrographs (final magnification 37,800× as determined from photographs of the grating replica) were then obtained from systematic randomly selected regions of pSR, dSR, and SLM of the same serial sections.

These electron micrographs were used to determine the number of immunogold particles per synapse, immunogold particle density per unit PSD area (μm^2), and identification of synaptic and MSB subtypes. Because all synapses analyzed in the present study were completely contained with each section series, the number of particles per synapse could be determined unequivocally by counting the total number of immunogold particles present on the PSD in all sections. For the analyses of receptor expression for synapses involved in a MSB, the first and last 3 sections of each series were eliminated from the analysis. This is a reasonable approach because we quantified the immunoexpression of synapses involved in MSBs, rather than their unbiased number, using the postembedding immunogold tissue. Particles were considered to be postsynaptic if they were projected onto the PSD, in the synaptic cleft, or otherwise within 20 nm of the PSD (Matsubara et al., 1996).

Antibody information

All antibodies are polyclonal, were obtained from Chemicon International (now part of Millipore, Bedford, MA), raised in rabbit, and affinity purified (Petralia and Wenthold, 1992; Wenthold et al., 1992; Petralia et al., 1994a, b). Antibodies to GluR1 (#AB1504, immunogen: C-terminus peptide sequence SHSSGMPLGATGL), GluR2 (#AB1768-25UG, immunogen: synthetic peptide from amino acids 827-842 of rat GluR2 conjugated to bovine serum albumin through a cysteine added to the C-terminus of the peptide), and GluR4 (#AB1508, immunogen: C-terminus peptide sequence RQSSGLAVIASDLP) all recognize a single band at the appropriate molecular weight upon Western blot analysis of rat brain and show no cross-reactivity with other glutamate receptor subunits. The antibody to GluR2/3 (#AB1506, immunogen: C-terminus of rat GluR2 peptide sequence EGYNVYGIESVKI, conjugated to bovine serum albumin with glutaraldehyde) recognizes both GluR2 and GluR3 on Western blot analysis of rat brain, but shows no cross-reaction with GluR1 or GluR4. The antibody to NR1 (#AB1516, immunogen: synthetic peptide sequence LQNQKDTVLPRRAIEREEGQLQLCSRHRES, corresponding to the C-terminus of rat NR1) recognizes a single band at ~ 120 kD on Western blot analysis of rat brain, and shows no cross-reaction with other glutamate receptor subunits. The NR2A/B antibody (#AB1548, immunogen: synthetic peptide LNSCSNRRVYKKMPSIESDV, corresponding to the C-terminus of rat NR2A conjugated to bovine serum albumin) recognizes both NR2A and NR2B equally on Western blot analysis of rat brain, with only the possibility of a very slight recognition of NR2C and NR2D. No cross reaction was seen with NR1 or other glutamate receptor subunits.

We labeled synapses with mixtures of primary antibodies to AMPAR and NMDAR subunits, because this is a standard method to maximize the labeling intensity, and it has been successfully used for quantification of the expression of these receptors at hippocampal synapses (Petralia et al., 1999, Takumi et al., 1999; Racca et al., 2000; Ganeshina et al., 2004a; Nicholson et al., 2006). It is possible that such approach involves a compromised efficiency of primary antibodies in the mixture. However, the benefit of improved overall labeling outweighs any possible deleterious effects of mixing the antibodies.

Digitization of electron micrographs

All electron micrograph negatives were scanned at 1200 dpi using a PowerLook 1100 scanner (Umax, Techville, TX) and printed with a HP Photosmart 7960 printer (Hewlett-

Packard, Palo Alto, CA) after adjustments to their tonal range using Photoshop 6.0 (Adobe Systems, Inc., San Jose, CA).

Statistical analyses

Differences among synaptic and MSB subtypes in pSR, dSR, and SLM were compared statistically using multivariate ANOVA and ANCOVA. When the analyses revealed significant main effects or interactions, means were compared with Tukey's Honestly Significant Difference post hoc test for samples with unequal numbers (significance was considered at $P < 0.05$). The variance of the data from individual rats was equivalent based on the results from Hartley's F Max test and Cochran's C test. Immunoexpression was compared with multivariate ANCOVA using PSD as the covariate. ANCOVA factors out the influence of the covariate (i.e., PSD area) on the parameter (i.e., immunogold particle number and density) and performs an ANOVA on the adjusted score (Maxwell and Delaney, 2004). In the absence of any true effect of either synaptic subtype or region, the results of the ANCOVA will result in means that are statistically equivalent. In other words, our statistical approach using multivariate ANCOVA factored out the influence of synapse size on receptor expression. Immunoreactivity among MSB synapses was compared first using ANOVA, with dendritic region and MSB subtype as factors. Subsequently, the immunoreactivity of perforated and nonperforated synapses was compared to their respective overall population using Welch's t-test with separate variance estimates and approximate/reduced degrees of freedom (Welch, 1938). The latter approach was taken as a conservative measure because the variance of the receptor expression levels (i.e., particle number) of MSB synapses was different from the overall population in both the AMPAR and NMDAR material.

RESULTS

We traced 361 perforated synapses and 546 nonperforated synapses to their parent dendrites in the conventional electron microscopic material, allowing us to unequivocally measure their spine volume and PSD area. This was not possible for the immunogold data, due to the low electron density of non-osmicated tissue. Therefore, all synapses whose PSDs were completely contained within the section series were analyzed for AMPAR and NMDAR immunoexpression. For the AMPAR experiments, 431 perforated and 1,306 immunopositive nonperforated synapses were analyzed. For the NMDAR immunogold study, we examined 356 perforated and 2,025 nonperforated synapses. The conventional electron microscopic MSB data derive from the analysis of 245 MSBs. AMPAR and NMDAR immunoreactivity was assessed in 79 and 92 MSBs, respectively.

Identification of synaptic subtypes in serial sections

Synapse morphology was extremely heterogeneous, but examining synapses in serial sections allowed us to categorize them unequivocally into the various subtypes of perforated and nonperforated synapses in the conventional and postembedding immunogold tissue (Tables 1-3).

The most numerous synaptic subtype was the nonperforated synapse (NP), with its characteristic disc-shaped, continuous PSD (Figs. 1A-E). The vast majority of NP synapses were small (PSD area < 0.04 μm^2), and when plotted in rank-order of PSD size showed an approximately linear distribution (Fig. 1F). This linearity ended, however, with synapses that were ~ 2 standard deviations (S.D.) larger than the mean NP PSD size (Fig. 1F). We interpreted this divergence from the linear pattern of PSD size as a reasonable and objective separation point for categorizing NP synapses as either “typical” NP synapses (i.e., those synapses whose PSD area was within 2 S.D. of the mean NP PSD area), or atypically large

NP synapses (ANP; i.e., those NP synapses with a PSD area > 2 S.D. above the mean; Figs. 2A-D). The lower end of the range for NP synapses also diverges from the linear trend, with the smaller NP synapses being slightly larger than what would be predicted. It is not clear whether or not this pattern has any significance, but it is important to note that NP synapses lacking AMPAR immunoreactivity are smaller on average than NP synapses that express AMPARs (Takumi et al., 1999; Nicholson et al., 2006).

The vast majority of typical NP synapses were located on thin spines with either no discernible head, or a spine head that was slightly rounded compared to its neck (Fig. 1A; out of 516 typical NP synapses in our conventional electron microscopic analysis, 461 were located on thin; 39 on sessile; and 16 on stubby spines). In contrast, ANP synapses were never found on thin spines (Figs. 2A-D; out of 30 ANPs in our conventional electron microscopic analysis, 28 were located on mushroom-shaped spines; 2 were located on sessile spines). In agreement with previous descriptions, spinules occasionally emanated from the spine heads of ANP synapses, and the cytoplasmic regions of their spines sometimes contained a spine apparatus (12/30 = 40%; see also Geinisman, 1993). Neither spinules nor spine apparati were found in typical NP synapses (0/516 = 0%). Another distinguishing feature of ANP synapses is that they always exhibited AMPAR expression (Fig. 2C), whereas ~40% of typical NP synapses lacked AMPAR immunoreactivity (Fig. 1D;Ganeshina et al., 2004a;Nicholson et al., 2006). Both NP (Fig. 1E) and ANP (Fig. 2D) synapses were always immunopositive for NMDARs.

Perforated synapses were less numerous, but still frequent, and could be distinguished from NP and ANP synapses by the presence of a discontinuity or perforation in their PSD. Most perforated synapses were located on mushroom-shaped spines (out of 361 perforated synapses, 310 of them were on mushroom-shaped spines; 24 were on stubby spines; 19 were on sessile spines; and 8 were on spines that were difficult to categorize morphologically; see also Harris and Stevens, 1989; Trommald and Hulleberg, 1997). By viewing these synapses in serial sections, we were able to categorize perforated synapses into three major subclasses: those with fenestrated (FP; Figs. 3A-D), horseshoe-shaped (HP; Figs. 4A-D), or segmented, completely partitioned (SCP; Figs. 5A-D) PSDs. A defining feature of perforated synapses is that their level of expression for both AMPARs and NMDARs exceeds that of NP synapses (compare Fig. 1 to Figs. 3-5). Additionally, SCP synapses were characterized by an abundance of immunogold particles for AMPARs, even compared to the other perforated synaptic subtypes (Ganeshina et al., 2004b; Fig. 5C).

FP, HP, and SCP synapses are all characterized by a substantially higher number and density of immunogold particles for AMPARs compared to their nonperforated counterparts. Both FP and HP synapses are different from SCP synapses, however, because the former are comprised of a single, albeit discontinuous, PSD; whereas the latter are comprised of multiple distinct PSD plates. Receptor expression in the FP and HP synapses did not differ (e.g., the average number of immunogold particles for AMPARs in pSR and dSR for FP synapses was 11.3 and 18.3, whereas that for HP synapses was 13.4 and 17.9, respectively), but both of these perforated synaptic subtypes differed from SCP synapses in that the AMPAR expression in the latter was significantly and markedly higher than in the former (see also Ganeshina et al., 2004b). Additionally, the PSDs of HP and FP synapses were smaller and they were located on smaller spines than those bearing SCP synapses. Though all perforated synaptic subtypes could be located on spines that contained a spine apparatus, the spines of SCP synapses were more likely to contain one (HP and FP: 72/260 = 27.7%; SCP: 80/101 = 79.2%). In view of the observation that FP and HP synapses did not differ with respect to their number, volume of their parent spines, PSD area, or level of immunoreactivity for AMPARs and NMDARs, we combined HP and FP synapses for

statistical comparisons into one group — other types of perforated (OP) synapses — to distinguish them from SCP synapses.

Synaptic subtype-specific scaling of number and size with distance from the soma

The high level of AMPAR expression that distinguishes SCP synapses from OP and NP synapses is consistent with the notion they are capable of generating very large synaptic potentials (Geinisman, 1993; Ganeshina et al., 2004b). The cable properties of CA1 pyramidal neuron dendrites affect synaptic potentials differently depending on where in the dendrite they are generated (Rall, 1967). For example, synaptic potentials generated in distal dendritic regions attenuate to a much larger degree as they propagate toward the soma/axon than those originating in more proximal locations (Rall, 1967). CA1 pyramidal neurons are known to compensate for this dendritic filtering by placing stronger synapses distally, which partially counteracts the voltage attenuation of distally-generated synaptic potentials (Magee and Cook, 2000; Nicholson et al., 2006; Spruston, 2008). We asked whether such distance-dependent synaptic scaling extended to SCP synapses specifically, or whether conductance scaling is effected simply by an increase in all perforated synaptic subtypes with distance from the soma.

Using unbiased stereological techniques, we found that SCP synapse number increased with distance from the soma, above and beyond that which occurs when all perforated synapses are pooled together (Nicholson et al., 2006; Fig. 6A). This perforated synaptic subtype-specific, distance-dependent increase was accomplished via a progressive upregulation in the proportion of SCP synapses as dendritic locations proceeded from pSR to dSR; and then from dSR to SLM (Figs. 6A, B). This pattern of results was confirmed statistically with a repeated measures ANOVA on the total number of OP and SCP synapses ($F_{(2,8)} = 6.332$) and on the SCP ratio ($F_{(2,4)} = 17.728$).

Receptor abundance is a major determinant of spine and synapse size (Nusser et al., 1998; Matsuzaki et al., 2001; Ganeshina et al., 2004a, 2004b; Nägerl et al., 2004; Zhou et al., 2004; Kopec et al., 2006, 2007). It is possible, however, that distal synapses and spines rely more heavily on circulating pools of proteins to maintain their structure and strength, rather than depending primarily on trafficking of such proteins from the soma. Competition for such molecules is likely to be high, which might confer an advantage to spines that are larger and therefore more diffusionally isolated (Koch and Zador, 1993; Bloodgood and Sabatini, 2005; Gray et al., 2006; Alvarez and Sabatini, 2007). To examine this notion directly, we measured the total spine volume and PSD area of those synapses whose parent spines could be traced to their parent dendrite.

SCP synapses were located on the largest spines and had the largest PSD areas, both of which increased progressively with distance from the soma (Figs. 6C, D; black triangles). Interestingly, both OP and ANP synapses and their spines also increased with distance from the soma (Figs. 6C, D; white triangles and black circles, respectively), whereas neither the PSD area nor the spine volume of typical NP synapses changed (Figs. 6C, D; white circles). These results were substantiated statistically using multivariate ANOVA, which revealed a significant region × subtype interaction for both spine volume ($F_{(6,896)} = 14.890$) and PSD area ($F_{(6,896)} = 20.951$).

The results from the conventional electron microscopic analysis show that spine and PSD size increases for synapses as they are located at progressively distal dendritic locations, but that this rule does not apply to typical NP synapses. Rather, NP synapses are remarkably invariant regardless of their dendritic location. Though it is possible that such size differences are indicative of the ability of distal synapses to self-regulate, it is also possible that such structural differences reflect changes in their expression level for synaptic

receptors. Therefore, we performed a similar synaptic subtype-specific examination using postembedding immunogold electron microscopy for AMPARs and NMDARs to determine whether differences exist in the various synaptic subtypes, and whether such differences are modified according to their dendritic location.

Synaptic subtype- and region-specific variability in AMPAR and NMDAR expression

Postembedding immunogold electron microscopy is currently the best available technique for localizing and quantifying synaptic protein expression, particularly for synaptic receptors (Ottersen and Landsend, 1997; Petralia and Wenthold, 1999; Nusser, 2000). Though ultrastructure is not as definitive as in conventional electron microscopy due to the absence of an osmication step, all synaptic subtypes could be distinguished unequivocally from one another in the AMPAR and NMDAR experiments (Figs. 1-5). As noted previously, all synapses were immunopositive for NMDARs, perforated and ANP synapses always expressed AMPARs, and the proportion of typical NP synapses lacking AMPAR immunoreactivity was ~40%, but did not differ with distance from the soma (Ganeshina et al., 2004a; Nicholson et al., 2006).

The AMPAR analysis involved all perforated synapses and only those nonperforated synapses with at least 1 immunogold particle projected onto their PSD profile (Ganeshina et al., 2004a; Nicholson et al., 2006). The results of this analysis indicated that there were both synaptic subtype-specific and dendritic region-specific differences. First, SCP synapses had the highest level of immunoexpression for AMPARs throughout SR, which was evident in the analysis of both immunogold particle number (Fig. 7A) and density (Fig. 7B). Secondly, immunoreactivity of SCP synapses showed an increase in dSR compared to pSR, but then decreased for synapses located in SLM (Figs. 7A, B). This pattern was also found to occur among OP synapses (Figs. 7A, B; see also Nicholson et al., 2006). And finally, ANP synapses had a higher number of immunogold particles for AMPARs than their smaller, typical NP counterparts, but an equivalent particle density (Figs. 7A, B). This suggests that ANP synapses have more AMPARs than typical NP synapses simply because they are bigger. Importantly, the level of AMPAR expression among ANP synapses was equal to that of OP synapses in pSR; and intermediate to that of typical NP and OP synapses in dSR and SLM. This pattern of results was confirmed with a multivariate ANCOVA, using PSD area as the covariate (region × subtype interaction; particle number: $F_{(6,1724)} = 37.055$; particle density: $F_{(6,1724)} = 15.020$).

The NMDAR analysis was undertaken to ascertain whether NMDAR expression also shows synaptic subtype-specific and region-specific differences. Furthermore, analysis of NMDAR expression among nonperforated synapses could clarify whether ANP synapses are simply large NP synapses, or whether they have an immunoexpression profile that is unlike typical NP synapses. In contrast to AMPAR expression, there was no evidence for regional differences in NMDAR immunoreactivity (Figs. 7C, D; see also Nicholson et al., 2006). Rather, the results showed that typical NP synapses had fewer immunogold particles for NMDARs and a higher particle density compared to all other synaptic subtypes, including ANP synapses. Statistical comparison of these synaptic subtype differences with a multivariate ANCOVA using PSD area as the covariate revealed a main effect of synaptic subtype, but no effect of dendritic region (particle number: $F_{(3,2368)} = 51.115$; particle density: $F_{(3,2368)} = 52.441$). These results show that the immunoexpression profile of ANP synapses is indeed different from that of typical NP synapses. Specifically, ANP synapses exhibit a NMDAR expression profile identical to that of both OP and SCP synapses (Figs. 7C, D) and an AMPAR expression profile intermediate to that of perforated and typical NP synapses (Figs. 7A, B).

Number of multiple synapse boutons

MSBs are structurally heterogeneous and can involve any combination of nonperforated and perforated axospinous synapses (Sorra and Harris, 1993). We used unbiased stereological counting procedures to estimate the total number of the different MSB subtypes and subsequently determined the receptor expression of their synapses with postembedding immunogold electron microscopy for AMPARs and NMDARs in pSR, dSR, and SLM.

The three types of axospinous MSB are those involving only nonperforated synapses (NP-NP; Fig. 8), those involving a mix of perforated and nonperforated synapses (P-NP; Fig. 9), and those involving exclusively perforated synapses (P-P; Fig. 10). The vast majority of MSBs we observed involved only 2 synapses (232/245 = 94.7%), while the remaining 5.3% (13/245) involved 3 synapses. Our unbiased estimates of total MSB number revealed that pSR had the most MSBs (Fig. 11A). When we classified MSBs into their subtypes, however, we found that the elevated MSB number in pSR was attributable to an increased frequency of MSBs involving only nonperforated synapses (i.e., NP-NP MSBs; Fig. 11B). Multivariate ANOVA of the total number of MSBs and their subtypes confirmed these observations (main effect of region: $F_{(2,18)} = 9.403$; region × subtype interaction: $F_{(4,18)} = 8.391$).

Receptor expression of synapses involved in multiple synapse boutons

Though the function of MSBs is unknown, one idea is that they provide a mechanism to increase coupling between presynaptic and postsynaptic neurons (Harris, 1995; Toni et al., 1999; Geinisman et al., 2001; Yankova et al., 2001). The main prediction of such a notion is that the synapses involved in a MSB will be of sufficient strength to contribute to neuronal output. Using serial section postembedding immunogold electron microscopy, we determined the expression of AMPARs and NMDARs in synapses making contact with a MSB. Though synaptic strength is most accurately estimated with local dendritic recordings and local stimulation (e.g., Magee and Cook, 2000), we feel that a reasonable and complementary approach is to infer synapse strength from the number of immunogold particles projected onto each synapse's PSD in serial sections. Such an approach enables us to estimate, at least grossly, the relative strength of synapses involved in the different types of MSB, from which inferences can be drawn regarding their relative efficacy (Nusser et al., 1998; Nicholson et al., 2006).

Overall, MSB synapses either showed low levels of expression for AMPARs and NMDARs, or were considerably disparate in their receptor expression (Figs. 12-14). Though there were significant differences in the pattern of receptor expression among synapses in the different MSB subtypes, statistical comparisons failed to finding any significant effects of distance from the soma (AMPAR: $F_{(4,70)} = 1.515$, $p = 0.207$; NMDAR: $F_{(4,83)} = 1.676$, $p = 0.163$). Therefore, the data from each MSB subtype were pooled across dendritic regions for statistical comparisons. To simplify the analysis, the number of immunogold particles for each synapse of an individual MSB was used to dichotomize synapses into those with more particles and those with fewer particles (Figs. 12-14). For MSBs with more than two synapses, the synapse with more immunogold particles was compared statistically to the average number of particles projected onto the synapses with fewer immunogold particles. As a conservative measure, we guarded against biasing the results by including MSBs with synapses containing an equivalent number of immunogold particles (including those that lacked AMPAR immunoreactivity).

Analysis of synaptic AMPAR expression showed that there are two main populations of NP-NP MSBs (Figs. 12A-C). The first subtype involved only NP synapses with few or no immunogold particles for AMPARs (Figs. 8B and C). Out of the 44 NP-NP MSBs in the

AMPAR material, 11 (25%) involved synapses with no more than 1 immunogold particle each (5 with all synapses lacking AMPAR immunoreactivity; 4 with at least 1 PSD lacking AMPAR immunoreactivity and the other(s) having only 1 immunogold particle; and 2 with each synapse having only 1 immunogold particle). The remaining 33 NP-NP MSBs (75%) comprised the second subtype, which was characterized by one (or more) NP synapse with a few or no immunogold particles and another NP synapse with more than 2 immunogold particles (Fig. 8D; 13 involved at least one synapse that completely lacked AMPAR immunoreactivity, with the remaining 20 involving at least one synapse with only 1 immunogold particle). NMDAR expression among synapses involved in a NP-NP MSB was generally consistent with, but less extreme than, the AMPAR experiment. Though all NP synapses exhibited NMDAR expression, 8 of the 49 NP-NP MSBs in the NMDAR material (16.3%) involved one synapse with 1 immunogold particle and another synapse with more than 2 immunogold particles (Fig. 8E). The remaining MSB synapses in the NP-NP MSB subtype all had more than 2 immunogold particles, but still showed a disparate pattern of receptor expression (Figs. 8F and 12D-F).

We next compared NP synapses involved in NP-NP MSBs to the overall population of NP synapses for the AMPAR and NMDAR experiments (including those NP synapses that lacked AMPAR immunoreactivity) using Welch's t-test with separate variance estimates and approximated/reduced degrees of freedom (Welch, 1938). First, the NP synapses containing the higher number of immunogold particles in each MSB had an elevated level of expression compared to the overall population for both AMPARs ($t_{(44.38)} = 3.030$; Fig. 12A) and NMDARs ($t_{(50.24)} = 7.576$; Fig. 12D). And second, NP synapses with the lower number of immunogold particles in each NP-NP MSB expressed significantly fewer AMPARs than would be expected from the overall population of NP synapses ($t_{(77.69)} = 10.612$; Fig. 12A). This pattern of results was also seen when each dendritic region was analyzed separately (Table 4). Taken together, these results show that NP-NP MSBs involve synapses that are either all abnormally weak (i.e., all synapses lack or show weak AMPAR immunoreactivity), or they involve one synapse that is unusually strong (i.e., it shows levels of AMPAR and NMDAR expression that exceeds what is typical of the NP synapse population) and another that is unusually weak.

Synapses involved in P-NP MSBs also showed great disparity in their expression for both AMPARs and NMDARs (Figs. 9B, C and 13 A-F), with perforated synapses usually having more, or occasionally the same number of, immunogold particles as compared to their NP synapse MSB partner. In the AMPAR experiment, many (13/32 = 40.6%) P-NP MSBs involved a perforated synapse with more than 8 immunogold particles and a NP synapse with zero (6/32) or one (7/32). Additionally, comparing synapses involved in a P-NP MSB to the overall population with Welch's t-test revealed that perforated synapses involved in a P-NP MSB have a higher number of immunogold particles for both AMPARs ($t_{(34.43)} = 2.647$; Fig. 13A) and NMDARs ($t_{(36.90)} = 3.523$; Fig. 13D) than the overall perforated synapse population. Neither the AMPAR nor the NMDAR expression of NP synapses involved in P-NP MSBs differed from the overall population of NP synapses. Thus, NP synapses involved in a P-NP MSB can be considered typical of the NP synapse population, but perforated synapses express an unusually high number of both AMPARs and NMDARs. Importantly, this pattern was also seen in each dendritic region (Table 4).

There was not a sufficient number of P-P MSBs to assess synaptic AMPAR expression reliably (n = 3; Figs. 14A-C), so no analyses were performed. There were, however, enough P-P MSBs in the NMDAR experiment to permit statistical comparisons (n = 9). As with both the NP-NP MSBs and the P-NP MSBs, there was considerable disparity in the immunoreactivity of the multiple perforated synapses making contact with the same presynaptic bouton (Figs. 14D-F). Statistical comparisons, using Welch's t-test, showed that

perforated synapses with the higher level of NMDAR expression for each P-P MSB are characterized by a level of NMDAR expression that exceeds that of the overall population of perforated synapses ($t_{(8.25)} = 2.920$; Fig. 14D). The perforated synapses with the lower level of NMDAR immunoreactivity from each P-P MSB were not significantly different from the overall population (Fig. 14D). Again, this pattern was evident in each dendritic region (Table 4). Importantly, however, given both the AMPAR and the NMDAR expression of the perforated synapses involved in the P-P MSBs, this MSB subtype, when activated, would likely be able to generate a significant amount of depolarization in each postsynaptic neuron or spine.

Together, these data suggest that only P-P MSBs allow a single presynaptic action potential to depolarize multiple postsynaptic neurons or spines to a significant degree. This subtype, however, was very rare (Fig. 11B; Sorra and Harris, 1993), so the vast majority of MSBs involve either only very weak synapses or one strong synapse and one (or more) very weak synapse.

DISCUSSION

The results of the present study show that there are both synaptic subtype-specific and dendritic region-specific differences in the number, size, receptor expression, and connectivity of axospinous synapses on hippocampal CA1 pyramidal neurons. First, the size and AMPAR expression of perforated synaptic subtypes changed with distance from the soma, whereas NP synapses showed neither changes in their receptor expression levels nor modifications in their size or spine morphology. An exception to this pattern among NP synapses was constrained to those NP synapses with atypically large PSDs. Such ANP synapses showed distance-dependent increases in PSD size as well as in spine size, similar to those found among the perforated synaptic subtypes. Second, both SCP and OP synapses increased in number with distance from the soma. Within SR, their AMPAR expression also increased in a distance-dependent manner, despite indistinguishable levels of NMDAR expression. Though SLM is the most distal dendritic region, the AMPAR expression of SCP and OP synapses was lower than that found among these synaptic subtypes in dSR. In contrast to the pattern of receptor expression of the perforated synaptic subtypes, there were no evident regional differences among the NP subtypes, including a lack of conductance scaling. Finally, MSBs were found to be most frequent in pSR, but only for those MSBs involving exclusively NP synapses. The synapses involved in a MSB, however, showed no differences across the dendritic regions with respect to their AMPAR and NMDAR expression. Regardless of their distance from the soma, there were two predominant patterns of receptor expression among MSB synapses: either all of the synapses expressed very few receptors, or one synapse expressed many and its counterparts expressed few. Some of the distance-dependent differences may reflect an increased reliance on synapses with an abundance of AMPARs to counteract the effects of dendritic filtering, whereas other differences may reflect an increased need to sequester circulating proteins. The disparity in the levels of receptor expression between synapses contacting the same presynaptic bouton suggest that the vast majority of MSBs in CA1 do not provide a means by which a single presynaptic action potential can cause significant depolarization in multiple neurons or spines.

Distance-dependent differences in synapses and their spines

All axospinous synaptic subtypes were found throughout the apical dendritic regions, but only typical NP synapses and their spines stayed the same size as they were located on progressively distal dendrites. Though ANP, OP, and SCP synapses all showed distance-dependent increases in size, only the OP and SCP synaptic subtypes exhibited parallel dendritic region-specific modifications in their number and AMPAR expression. NMDAR

expression, on the other hand, did not change with distance from the soma, but ANP, OP, and SCP synapses all had more immunogold particles for NMDARs than NP synapses.

Our results are consistent with the notion that the increase in the number and strength of SCP synapses in SR acts as a compensatory mechanism to counteract voltage attenuation. The AMPAR expression differences between SCP and OP synapses disappear in SLM, suggesting that unitary synaptic conductances are unable to compensate for their distance from the soma in this region, and probably contribute to action potential output primarily through a different mechanism (e.g., contributing to dendritic spikes; Jarsky et al., 2005; Nicholson et al., 2006; Spruston, 2008). That NMDAR expression does not change with distance from the soma is consistent with previous results (Nicholson et al., 2006). The identification of a unique expression profile for ANP synapses, however, has not been described previously. Furthermore, this expression profile suggests that ANP synapses are a synaptic subtype in and of themselves, and is consistent with the notion that they are structural and immunocytochemical intermediates in activity-dependent synaptic cycling (Geinisman, 1993). Finally, the observation that ANP, OP, and SCP synapses showed similar changes in their structure with distance from the soma suggests that these synaptic subtypes are regulated differently from typical NP synapses, which did not change in size, structure, or strength.

Recent evidence indicates that small spines show more and longer-lasting plasticity than larger spines (Matsuzaki et al., 2004; Lang et al., 2005; Noguchi et al., 2005). Other studies have reported that spines that could be repeatedly imaged over multiple days/weeks were invariably large, but that small, thin spines were only visible for a day or two (Trachtenberg et al., 2002; Holtmaat et al., 2005; Knott et al., 2006). The volumes for large, stable spines and small, transient ones reported in these studies correspond closely with the volumes we report in this study for OP and SCP synapse-bearing spines and NP synapse-bearing spines, respectively.

It is reasonable, therefore, to suggest that large spines bearing either OP or SCP synapses are more stable and more mature than smaller spines bearing NP synapses (see also Kasai et al., 2003; Bourne and Harris, 2007, 2008). Furthermore, SCP synapses, with their large volumes and abundance of AMPARs, may be self-sustaining by generating large currents confined to their spine heads (Segev and Rall, 1988; Tsay and Yuste, 2004; Spruston, 2008), which are capable of activating signal transduction cascades and stabilizing the actin cytoskeleton (Bloodgood & Sabatini, 2005). These results suggest that SCP and OP synapses could be a source of persistent and invariant information for CA1 pyramidal neurons (e.g., place fields). Such a notion is consistent with our previous study (Nicholson et al., 2004), which found that aged rats with impaired spatial learning exhibited a dramatic reduction in the size of their OP and SCP synapses, but not their NP synapses.

It has been suggested that SCP synapses are especially efficacious on the basis of their transient increase during early phases of long-term potentiation (Geinisman et al., 1993; Toni et al., 2001) and on their AMPAR immunoreactivity (Ganeshina et al., 2004b). That the number and level of AMPAR expression increased between pSR and dSR within SCP synapses is consistent with the idea that perforated synapses play a pivotal role in counteracting voltage attenuation of synaptic potentials as they propagate toward the soma (Nicholson et al., 2006; Spruston, 2008). Why their number is highest in SLM is unknown, however, particularly because neither their AMPAR nor NMDAR immunoreactivity was different from that of OP synapses in this region. Future studies are needed to address whether synaptic transmission is different at SCP synapses as compared to OP, ANP, or NP synapses. For example, the presence of spine partitions and multiple release zones suggests the intriguing possibility that multiquantal release occurs frequently at SCP synapses, which

may act to saturate the high number of AMPARs of these synapses and consequently generate large local potentials (Geinisman, 1993; Conti and Lisman, 2003; Raghavachari and Lisman, 2004). Within pSR and dSR, the large potentials originating at SCP synapses may successfully overcome voltage attenuation and depolarize the soma. Within SLM, however, a premium might be placed on the hypothesized multiquantal nature of synaptic transmission at SCP synapses, rather than synaptic strength per se, because their AMPAR immunoreactivity is the same as those in pSR, but they are 6-times more frequent.

The functional implications of the distance-dependent increases in PSD and spine morphology in all but the NP synapses are also unknown. Within SR, this could be attributable to the accommodation of the higher number of AMPARs found in OP and SCP synapses in dSR. This reasoning, however, does not explain the continued increase in synapse and spine size in SLM, where AMPAR expression is the same as that in pSR among OP and SCP synapses. Similarly, the size of ANP synapses and their spines also increases with distance from the soma, whereas their AMPAR immunoreactivity does not. Rather, the distance-dependent increase in the size of synapses and their spines is more consistent with the notion that self-reliance is necessary for survival in distal dendritic regions. Because synapses located on large spines can be diffusionally isolated from their parent dendrites (Koch and Zador, 1993; Svoboda et al., 1996; Bloodgood and Sabatini, 2005; Alvarez and Sabatini, 2007), OP and SCP synapses may be more capable of self-regulation than their smaller, nonperforated counterparts.

A possible role for multiple synapse boutons in CA1

All synaptic subtypes were represented in the synapses that formed MSBs, but only MSBs involving exclusively NP synapses showed any regional differences, with their number being highest in pSR. The central hypothesis tested was that MSBs are a mechanism by which a single presynaptic action potential can produce excitatory postsynaptic potentials in multiple neurons or spines. When the strength of each synapse was estimated using postembedding immunogold electron microscopy for AMPARs and NMDARs, however, there was only one MSB subtype that would likely be able to perform such a function. The MSB subtype comprised exclusively of perforated synapses (i.e., P-P MSB) involved synapses that had either a level of AMPAR and NMDAR expression typical of perforated synapses, or a level that exceeded their overall population mean. Assuming that synaptic strength correlates with AMPAR number, and that immunolocalization in the present study provided an accurate estimate of the relative abundance of both AMPARs and NMDARs, the synapses comprising P-P MSBs would likely be of sufficient strength to produce a significant local and somatic depolarization (Nicholson et al., 2006; Spruston, 2008). The other MSB subtypes generally had synapses with no or just a few immunogold particles for AMPARs and NMDARs; or had one synapse with many immunogold particles for AMPARs and NMDARs and another (or more) with few or none. Given that the P-P MSBs are rare (they comprise only about 2.9% of the MSB population), it is unlikely that generating simultaneous local depolarizations is the primary function of MSBs. Rather, our data are more consistent with the notion that most MSBs may be transient, and involve at least one newly formed synapse (see also Woolley et al., 1996; Toni et al., 2007). Spine motility and turnover are found primarily among small, thin spines (Trachtenberg et al., 2002; Holtmaat et al., 2005; Knott et al., 2006). Therefore, MSBs may be created de novo as either NP-NP or P-NP MSBs (see also Woolley et al., 1996; Toni et al., 2007), whereas P-P MSBs may either be structurally stable or in the process of converting back into one of the other two MSB subtypes.

Many MSBs may therefore be targets of competition between synapses, rather than mechanisms that multiply efficacious synapses. Such a notion is consistent with previous results because many of the conditions that increase MSB number could also be expected to

increase competition among synapses for functional or relevant inputs. For example, MSBs increase in frequency after exposure to conditions that induce reactive or recuperative synaptogenesis including partial deafferentation (Steward et al., 1988; Hatton, 1990; Jones, 1999; Meshul et al., 2000), visual deprivation (Friedlander et al., 1991), hormonal treatments (Woolley et al., 1996; Yankova et al., 2001), and vibratome slicing of live tissue (Kirov et al., 1999). Furthermore, MSBs are involved in plasticity associated with learning new motor skills (Jones et al., 1999; Federmeier et al., 2002), environmental enrichment (Jones et al., 1997), acquisition of trace eyeblink conditioning (Geinisman et al., 2001), induction of long-term potentiation (Toni et al., 1999), and neurogenesis (Toni et al., 2007). All of these conditions are associated with a transient increase in competition among synapses for a presynaptic partner, and we propose that MSBs provide a mechanism by which synaptic reorganization can be achieved without necessarily resulting in net synaptogenesis (Geinisman et al., 2001).

Synaptic reorganization can involve the addition of new, active synapses and the removal of inactive ones. Or, it can entail the conversion of the weaker synaptic subtypes into the stronger ones (or vice versa). For example, synaptic potentials originating at typical NP synapses are not likely to propagate to the soma/axon, whereas those originating at perforated synapses are (Nicholson et al., 2006; Spruston, 2008). If a NP synapse is converted by activity into an OP or SCP synapse, however, this would result in a new functional synapse without requiring synaptogenesis. The “synaptic cycling hypothesis” posits that the bidirectional transition between NP synapses and perforated synapses is driven by changes in the level of synaptic activity (Nieto-Sampedro et al., 1982; Carlin and Siekevitz, 1983; Geinisman, 1993; Bourne and Harris, 2007). Though such changes can be influenced by presynaptic factors like quantal content, the availability of synaptic receptors to bind released glutamate is the primary determinant of synaptic strength (Lüscher et al., 2000; Malinow and Malenka, 2002; Bredt and Nicoll, 2003; Malenka and Bear, 2004). Such a view posits that, provided presynaptic parameters remain stable, receptor insertion increases synaptic strength, whereas receptor removal decreases it. If most MSBs are host to synapses that are in competition with each other, as the disparate pattern of receptor expression between synapses contacting the same MSB suggests, then this competition may end when one synapse converts from a weak subtype (e.g., NP synapse) into a strong one (e.g., OP or SCP synapse), ultimately becoming the sole target of that presynaptic bouton.

Presynaptic structural changes notwithstanding, the competition among MSB synapses is likely to occur over a time scale of hours to days, whereas the formation of a MSB may occur relatively rapidly due to new spine outgrowth or spine motility (Woolley et al., 1996; Toni et al., 1999; Trachtenberg et al., 2002; Holtmaat et al., 2005; Knott et al., 2006). Additionally, the spine motility and outgrowth that is found primarily among thin spines (Trachtenberg et al., 2002; Holtmaat et al., 2005; Knott et al., 2006), which we found only have NP synapses, provides a mechanism to replace NP synapses that are eliminated during competition at MSBs (at the same or a different dendritic location). The replenishment of NP synapses by these two processes therefore results in neither synaptogenesis nor synapse loss.

Importantly, it is also possible that the weaker synapses on MSBs are neither transient nor in competition with the other synapses contacting that MSB. Rather, these weaker synapses may remain in place despite their low level or lack of AMPAR immunoreactivity. In such a scenario, each MSB may have the potential for activity-dependent conversion into a P-P MSB, which would indeed increase coupling between the presynaptic bouton and the postsynaptic spines (Harris, 1995; Toni et al., 1999).

Conclusions

We have shown here that it is only the perforated synaptic subtypes (i.e., OP and SCP synapses) that show increases in their number and changes in their receptor expression with distance from the soma. Though ANP synapses and their spines showed morphological changes paralleling those seen among OP and SCP synapses, their receptor expression showed no evidence of conductance scaling. We previously found that NP synapse number does not differ between pSR and dSR, but is lowest in SLM (Nicholson et al., 2006). In each case, however, they are still by far the most numerous (~80% of the total population of axospinous synapses). Yet, the NP synaptic subtype showed variation in neither its size nor its receptor expression across the apical dendritic regions. The underlying mechanisms responsible for this pattern of synapse-specific regulation are unknown, but it is possible that they reflect an increased need for conductance scaling and protein sequestration in distal dendritic regions, as well as the enduring need for synaptogenesis/reorganization that the pool of NP synapses may provide. The function of MSBs also remains unknown, but the data presented here are inconsistent with the notion that their primary function is to generate significant depolarization in multiple neurons or spines. Rather, the pattern of AMPAR and NMDAR expression among synapses comprising an individual MSB show that MSB synapses are either all unusually weak, or involve a relatively weak one and an unusually strong one.

Acknowledgments

This work was supported by National Institute on Aging grants P30 AG013854 to the Northwestern University Alzheimer's Disease Core Center, T32 AG020506 and K99 AG031574 (to D.A.N.), and R01 AG017139 (to Y.G.). We thank Nelson Spruston for helpful discussions.

Grant sponsor: National Institutes of Health; Grant numbers: T32 AG20506; P30 AG013854; K99 AG031574 (to D.A.N.) and R01 AG017139 (to Y.G.).

LITERATURE CITED

Alvarez VA, Sabatini BL. Anatomical and physiological plasticity of dendritic spines. Annu Rev Neurosci. 2007; 30:79–97. [PubMed: 17280523]

Bloodgood BL, Sabatini BL. Neuronal activity regulates diffusion across the neck of dendritic spines. Science. 2005; 310:866–869. [PubMed: 16272125]

Bourne J, Harris KM. Do thin spines learn to be mushroom spines that remember? Curr Opin Neurobiol. 2007; 17:381–386. [PubMed: 17498943]

Bourne JN, Harris KM. Balancing structure and function at hippocampal dendritic spines. Annu Rev Neurosci. 2008; 31:47–67. [PubMed: 18284372]

Bredt DS, Nicoll RA. AMPA receptor trafficking at excitatory synapses. Neuron. 2003; 40:361–379. [PubMed: 14556714]

Calverley RK, Jones DG. Contributions of dendritic spines and perforated synapses to synaptic plasticity. Brain Res Brain Res Rev. 1990; 15:215–249. [PubMed: 2289086]

Carlin RK, Siekevitz P. Plasticity in the central nervous system: do synapses divide? Proc Natl Acad Sci USA. 1983; 80:3517–3521. [PubMed: 6574496]

Cohen RS, Siekevitz P. Form of the postsynaptic density. A serial section study. J Cell Biol. 1978; 78:36–46. [PubMed: 670296]

Colonnier M. Synaptic patterns on different cell types in the different laminae of the cat visual cortex. An electron microscope study. Brain Res. 1968; 9:268–287. [PubMed: 4175993]

Conti R, Lisman J. The high variance of AMPA receptor- and NMDA receptor-mediated responses at single hippocampal synapses: evidence for multiquantal release. Proc Natl Acad Sci USA. 2003; 100:4885–4890. [PubMed: 12682300]

Desmond NL, Weinberg RJ. Enhanced expression of AMPA receptor protein at perforated axospinous synapses. Neuroreport. 1998; 9:857–860. [PubMed: 9579679]

Dyson SE, Jones DG. Synaptic remodeling during development and maturation: junction differentiation and splitting as a mechanism for modifying connectivity. Brain Res. 1984; 315:125–137. [PubMed: 6722573]

Eichenbaum H, Harris KM. Toying with memory in the hippocampus. Nat Neurosci. 2000; 3:205–206. [PubMed: 10700247]

Federmeier KD, Kleim JA, Greenough WT. Learning-induced multiple synapse formation in cerebellar cortex. Neurosci Lett. 2002; 332:180–184. [PubMed: 12399010]

Fiala JC. Reconstruct: a free editor for serial section microscopy. J Microsc. 2005; 218:52–61. [PubMed: 15817063]

Friedlander MJ, Martin KAC, Wassenhove-McCarthy D. Effects of monocular visual deprivation on geniculocortical innervation of area 18 in cat. J Neurosci. 1991; 11:3268–3288. [PubMed: 1941084]

Funke L, Dakoji S, Bredt DS. Membrane-associated guanylate kinases regulate adhesion and plasticity at cell junctions. Annu Rev Biochem. 2005; 74:219–245. [PubMed: 15952887]

Ganeshina O, Berry RW, Petralia RS, Nicholson DA, Geinisman Y. Differences in the expression of AMPA and NMDA receptors between axospinous perforated and nonperforated synapses are related to the configuration and size of postsynaptic densities. J Comp Neurol. 2004a; 468:86–95. [PubMed: 14648692]

Ganeshina O, Berry RW, Petralia RS, Nicholson DA, Geinisman Y. Synapses with a segmented, completely partitioned postsynaptic density express more AMPA receptors than other axospinous synaptic junctions. Neuroscience. 2004b; 125:615–623. [PubMed: 15099675]

Geinisman Y. Perforated axospinous synapses with multiple, completely partitioned transmission zones: probably structural intermediates in synaptic plasticity. Hippocampus. 1993; 3:417–433. [PubMed: 8269034]

Geinisman Y. Structural synaptic modifications associated with hippocampal LTP and behavioral learning. Cereb Cortex. 2000; 10:952–962. [PubMed: 11007546]

Geinisman Y, Berry RW, Disterhoft JF, Power JM, Van der Zee EA. Associative learning elicits the formation of multiple-synapse boutons. J Neurosci. 2001; 21:5568–5573. [PubMed: 11466428]

Geinisman Y, de Toledo-Morrell L, Morrell F. Aged rats need a preserved complement of perforated axospinous synapses per hippocampal neuron to maintain good spatial memory. Brain Res. 1986; 398:266–275. [PubMed: 3801904]

Geinisman Y, de Toledo-Morrell L, Morrell F, Heller RE, Rossi M, Parshall RF. Structural synaptic correlate of long-term potentiation: formation of axospinous synapses with multiple,completely partitioned transmission zones. Hippocampus. 1993; 3:435–445. [PubMed: 8269035]

Geinisman Y, Disterhoft JF, Hundersen HJ, McEchron MD, Persina IS, Power JM, Van der Zee EA, West MJ. Remodeling of hippocampal synapses after hippocampus-dependent associative learning. J Comp Neurol. 2000; 417:49–59. [PubMed: 10660887]

Geinisman Y, Ganeshina O, Yoshida R, Berry RW, Disterhoft JF, Gallagher M. Aging,spatial learning, and total synapse number in the rat CA1 stratum radiatum. Neurobiol Aging. 2004; 25:407–416. [PubMed: 15123345]

Geinisman Y, Gundersen HJ, Van der Zee EA, West MJ. Unbiased stereological estimation of the total number of synapses in a brain region. J Neurocytol. 1996; 25:805–819. [PubMed: 9023726]

Geinisman Y, Morrell F, de Toledo-Morrell L. Axospinous synapses with segmented postsynaptic densities: a morphologically distinct synaptic subtype contributing to the number of profiles of ‘perforated’ synapses. Brain Res. 1987; 423:179–188. [PubMed: 3676805]

Gray EG. Electron microscopy of synaptic contacts on dendrite spines of the cerebral cortex. Nature. 1959; 183:1592–1593. [PubMed: 13666826]

Gray NW, Weimer RM, Bureau I, Svoboda K. Rapid redistribution of synaptic PSD-95 in the neocortex in vivo. PLoS Biol. 2006; 4:e370. [PubMed: 17090216]

Harris KM, Stevens JK. Dendritic spines of CA1 pyramidal cells in rat hippocampus:serial section electron microscopy with reference to their biophysical characteristics. J Neurosci. 1989; 9:2982–2997. [PubMed: 2769375]

Harris KM, Kater SB. Dendritic spines: cellular specializations imparting both stability and flexibility to synaptic function. Annu Rev Neurosci. 1994; 17:341–371. [PubMed: 8210179]

Harris KM. How multiple-synapse boutons could preserve input specificity during an interneuronal spread of LTP. Trends Neurosci. 1995; 18:365–369. [PubMed: 7482800]

Hatton GI. Emerging concepts of structure-function dynamics in adult brain: the hypothalamo-neurohypophysial system. Prog Neurobiol. 1990; 34:437–504. [PubMed: 2202017]

Hayashi Y, Majewska AK. Dendritic spine geometry: functional implication and regulation. Neuron. 2005; 46:529–532. [PubMed: 15944122]

Holtmaat AJ, Trachtenberg JT, Wilbrecht L, Shepherd GM, Zhang X, Knott GW, Svoboda K. Transient and persistent dendritic spines in the neocortex in vivo. Neuron. 2005; 45:279–291. [PubMed: 15664179]

Jarsky T, Roxin A, Kath WL, Spruston N. Conditional dendritic spike propagation following distal synaptic activation of hippocampal CA1 pyramidal neurons. Nat Neurosci. 2005; 8:1667–1776. [PubMed: 16299501]

Jones DG, Harris RJ. An analysis of contemporary morphological concepts of synaptic remodeling in the CNS: perforated synapses revisited. Rev Neurosci. 1995; 6:177–219. [PubMed: 8717635]

Jones TA. Multiple synapse formation in the motor cortex opposite unilateral sensorimotor cortex lesions in adult rats. J Comp Neurol. 1999; 414:57–66. [PubMed: 10494078]

Jones TA, Chu CJ, Grande LA, Gregory AD. Motor skills training enhances lesion-induced structural plasticity in the motor cortex of adult rats. J Neurosci. 1999; 19:10153–10163. [PubMed: 10559423]

Jones TA, Klintsova AY, Kilman VL, Sirevaag AM, Greenough WT. Induction of multiple synapses by experience in the visual cortex of adult rats. Neurobiol Learn Mem. 1997; 68:13–20. [PubMed: 9195585]

Kasai H, Matsuzaki M, Noguchi J, Yasumatsu N, Nakahara H. Structure-stability-function relationships of dendritic spines. Trends Neurosci. 2003; 26:360–368. [PubMed: 12850432]

Kennedy MB. Signal-processing machines at the postsynaptic density. Science. 2000; 290:750–754. [PubMed: 11052931]

Kennedy MB, Beale HC, Carlisle HJ, Washburn LR. Integration of biochemical signaling in spines. Nat Rev Neurosci. 2005; 6:423–434. [PubMed: 15928715]

Kim E, Sheng M. PDZ domain proteins of synapses. Nat Rev Neurosci. 2004; 5:771–781. [PubMed: 15378037]

Kirov SA, Sorra KE, Harris KM. Slices have more synapses than perfusion-fixed hippocampus from both young and mature rats. J Neurosci. 1999; 19:2876–2886. [PubMed: 10191305]

Knott GW, Holtmaat A, Wilbrecht L, Welker E, Svoboda K. Spine growth precedes synapse formation in the adult neocortex in vivo. Nat Neurosci. 2006:1117–1124. [PubMed: 16892056]

Koch C, Zador A. The function of dendritic spines: devices subserving biochemical rather than electrical compartmentalization. J Neurosci. 1993; 13:413–422. [PubMed: 8426220]

Kopec CD, Li B, Wei W, Boehm J, Malinow R. Glutamate receptor exocytosis and spine enlargement during chemically induced long-term potentiation. J Neurosci. 2006; 26:2000–2009. [PubMed: 16481433]

Kopec CD, Real E, Kessels HW, Malinow R. GluR1 links structural and functional plasticity at excitatory synapses. J Neurosci. 2007; 27:13706–13718. [PubMed: 18077682]

Lang C, Barco A, Zablow L, Kandel ER, Siegelbaum SA, Zakharenko SS. Transient expansion of synaptically connected dendritic spines upon induction of hippocampal long-term potentiation. Proc Natl Acad Sci USA. 2004; 101:16665–16670. [PubMed: 15542587]

London M, Häusser M. Dendritic computation. Annu Rev Neurosci. 2005; 28:503–532. [PubMed: 16033324]

Lüscher C, Nicoll RA, Malenka RC, Muller D. Synaptic plasticity and dynamic modulation of the postsynaptic membrane. Nat Neurosci. 2000; 3:545–550. [PubMed: 10816309]

Magee JC, Cook EP. Somatic EPSP amplitude is independent of synapse location in hippocampal pyramidal neurons. Nat Neurosci. 2000; 3:895–903. [PubMed: 10966620]

Malenka RC, Bear MF. LTP and LTD: an embarrassment of riches. Neuron. 2004; 44:5–21. [PubMed: 15450156]

Malinow R, Malenka RC. AMPA receptor trafficking and synaptic plasticity. Annu Rev Neurosci. 2002; 25:103–126. [PubMed: 12052905]

Matsubara A, Laake JH, Davanger S, Usami S, Ottersen OP. Organization of AMPA receptor subunits at a glutamate synapse: a quantitative immunogold analysis of hair cell synapses in the rat organ of Corti. J Neurosci. 1996; 16:4457–4467. [PubMed: 8699256]

Matsuzaki M, Ellis-Davies GC, Nemoto T, Miyashita Y, Iino M, Kasai H. Dendritic spine geometry is critical for AMPA receptor expression in hippocampal CA1 pyramidal neurons. Nat Neurosci. 2001; 4:1086–1092. [PubMed: 11687814]

Matsuzaki M, Honkura N, Ellis-Davies GC, Kasai H. Structural basis of long-term potentiation in single dendritic spines. Nature. 2004; 429:761–766. [PubMed: 15190253]

Maxwell, SE.; Delaney, HD. Designing experiments and analyzing data: a model comparison perspective. 2nd Ed. Lawrence Erlbaum Associates; Mahwah, NJ: 2004.

Meshul CK, Cogen JP, Cheng HW, Moore C, Krentz L, McNeill TH. Alterations in rat striatal glutamate synapses following a lesion of the cortico- and/or nigrostrial pathway. Exp Neurol. 2000; 165:191–206. [PubMed: 10964498]

Muller D. Ultrastructural plasticity of excitatory synapses. Rev Neurosci. 1997; 8:77–93. [PubMed: 9344180]

Nägerl UV, Eberhorn N, Cambridge SB, Bonhoeffer T. Bidirectional activity-dependent morphological plasticity in hippocampal neurons. Neuron. 2004; 44:759–767. [PubMed: 15572108]

Nicholson DA, Trana R, Katz Y, Kath WL, Spruston N, Geinisman Y. Distance-dependent differences in synapse number and AMPA receptor expression in hippocampal CA1 pyramidal neurons. Neuron. 2006; 50:431–442. [PubMed: 16675397]

Nicholson DA, Yoshida R, Berry RW, Gallagher M, Geinisman Y. Reduction in size of perforated postsynaptic densities in hippocampal axospinous synapses and age-related spatial learning impairments. J Neurosci. 2004; 24:7648–7653. [PubMed: 15342731]

Nieto-Sampedro M, Hoff SF, Cotman CW. Perforated postsynaptic densities: probable intermediates in synapse turnover. Proc Natl Acad Sci USA. 1982; 79:5718–5722. [PubMed: 6957887]

Nimchinsky EA, Sabatini BL, Svoboda K. Structure and function of dendritic spines. Annu Rev Physiol. 2002; 64:313–353. [PubMed: 11826272]

Noguchi J, Matsuzaki M, Ellis-Davies GC, Kasai H. Spine-neck geometry determines NMDA receptor-dependent Ca^{2+}signaling in dendrites. Neuron. 2005; 46:609–622. [PubMed: 15944129]

Nusser Z. AMPA and NMDA receptors: similarities and differences in their synaptic distribution. Curr Opin Neurobiol. 2000; 10:337–341. [PubMed: 10851167]

Nusser Z, Lujan R, Laube G, Roberts JD, Molnar E, Somogyi P. Cell type and pathway dependence of synaptic AMPA receptor number and variability in the hippocampus. Neuron. 1998; 21:545–559. [PubMed: 9768841]

Ottersen OP, Landsend AS. Organization of glutamate receptors at the synapse. Eur J Neurosci. 1997; 9:2219–2224. [PubMed: 9464917]

Peters A, Kaiserman-Abramof IR. The small pyramidal neuron of the rat cerebral cortex. The synapses upon dendritic spines. Z Zellforsch Mikrosk Anat. 1969; 100:487–506. [PubMed: 5351190]

Peters A, Kaiserman-Abramof IR. The small pyramidal neuron of the rat cerebral cortex. The perikaryon, dendrites, and spines. Am J Anat. 1970; 127:321–355. [PubMed: 4985058]

Petralia RS, Esteban JA, Wang YX, Partridge JG, Zhao HM, Wenthold RJ, Malinow R. Selective acquisition of AMPA receptors over postnatal development suggests a molecular basis for silent synapses. Nat Neurosci. 1999; 2:31–36. [PubMed: 10195177]

Petralia RS, Yokotani N, Wenthold RJ. Light and electron microscope distribution of the NMDA receptor subunit NMDAR1 in the rat nervous system using a selective anti-peptide antibody. J Neurosci. 1994a; 14:667–696. [PubMed: 8301357]

Petralia RS, Wang YX, Wenthold RJ. The NMDA receptor subunits NR2A and NR2B show histological and ultrastructural localization patterns similar to those of NR1. J Neurosci. 1994b; 14:6102–6120. [PubMed: 7931566]

Petralia RS, Wenthold RJ. Light and electron immunocytochemical localization of AMPA-selective glutamate receptors in the rat brain. J Comp Neurol. 1992; 318:329–354. [PubMed: 1374769]

Petralia RS, Wenthold RJ. Immunocytochemistry of NMDA receptors. Methods Mol Biol. 1999; 128:73–92. [PubMed: 10320974]

Racca C, Stephenson FA, Streit P, Roberts JD, Somogyi P. NMDA receptor content of synapses in stratum radiatum of the hippocampal CA1 area. J Neurosci. 2000; 20:2512–2522. [PubMed: 10729331]

Raghavachari S, Lisman JE. Properties of quantal transmission at CA1 synapses. J Neurophysiol. 2004; 92:2456–2467. [PubMed: 15115789]

Rall W. Distinguishing theoretical synaptic potentials computed for different somadendritic distributions of synaptic input. J Neurophysiol. 1967; 30:1138–1168. [PubMed: 6055351]

Scannevin RH, Huganir RL. Postsynaptic organization and regulation of excitatory synapses. Nat Rev Neurosci. 2000; 1:133–141. [PubMed: 11252776]

Segev I, Rall W. Computational study of an excitable dendritic spine. J Neurophysiol. 1988; 60:499–523. [PubMed: 2459320]

Sheng M, Hoogenraad CC. The postsynaptic architecture of excitatory synapses: a more quantitative view. Annu Rev Biochem. 2007; 76:823–847. [PubMed: 17243894]

Sjöström PJ, Rancz EA, Roth A, Häusser M. Dendritic excitability and synaptic plasticity. Physiol Rev. 2008; 88:769–840. [PubMed: 18391179]

Smith MA, Ellis-Davies GC, Magee JC. Mechanism of the distance-dependent scaling of Schaffer collateral synapses in rat CA1 pyramidal neurons. J Physiol. 2003; 548:245–258. [PubMed: 12598591]

Sorra KE, Harris KM. Occurrence and three-dimensional structure of multiple synapses between individual radiatum axons and their target pyramidal cells in hippocampal area CA1. J Neurosci. 1993; 13:3736–3748. [PubMed: 8366344]

Spacek J, Hartmann M. Three-dimensional analysis dendritic spines. I. Quantitative observations related to dendritic spine synaptic morphology in cerebral and cerebellar cortices. Anat Embryol (Berl). 1983; 167:289–310. [PubMed: 6614508]

Spruston N. Pyramidal neurons: dendritic structure and synaptic integration. Nat Rev Neurosci. 2008; 9:206–221. [PubMed: 18270515]

Steward O, Vinsant SL, Davis L. The process of reinnervation in the dentate gyrus of adult rats: an ultrastructural study of changes in presynaptic terminals as a result of sprouting. J Comp Neurol. 1988; 267:203–210. [PubMed: 3343397]

Svoboda K, Tank DW, Denk W. Direct measurement of coupling between dendritic spines and shafts. Science. 1996; 272:716–719. [PubMed: 8614831]

Takumi Y, Ramirez-León V, Laake P, Rinvik E, Ottersen OP. Different modes of expression of AMPA and NMDA receptors in hippocampal synapses. Nat Neurosci. 1999; 2:618–624. [PubMed: 10409387]

Toni N, Buchs PA, Nikonenko I, Bron CR, Muller D. LTP promotes formation of multiple spine synapses between a single axon terminal and a dendrite. Nature. 1999; 402:421–425. [PubMed: 10586883]

Toni N, Buchs PA, Nikonenko I, Povilaitite P, Parisi L, Muller D. Remodeling of synaptic membranes after induction of long-term potentiation. J Neurosci. 2001; 21:6245–6251. [PubMed: 11487647]

Toni N, Teng EM, Bushong EA, Aimone JB, Zhao C, Consiglio A, van Praag H, Martone ME, Ellisman MH, Gage FH. Synapse formation on neurons born in the adult hippocampus. Nat Neurosci. 2007; 10:727–734. [PubMed: 17486101]

Trachtenberg JT, Chen BE, Knott GW, Feng G, Sanes JR, Welker E, Svoboda K. Long-term in vivo imaging of experience-dependent synaptic plasticity in adult cortex. Nature. 2002; 420:788–794. [PubMed: 12490942]

Trommald M, Hulleberg G. Dimensions and density of dendritic spines from rat dentate granule cells based on reconstructions from serial electron micrographs. J Comp Neurol. 1997; 377:15–28. [PubMed: 8986869]

Tsay D, Yuste R. On the electrical function of dendritic spines. Trends Neurosci. 2004; 27:77–83. [PubMed: 15102486]

Welch BL. The significance of the differences between two means when the population variances are unequal. Biometrika. 1938; 29:350–362.

Wenthold RJ, Yokotani N, Doi K, Wada K. Immunochemical characterization of the non-NMDA glutamate receptor using subunit-specific antibodies. Evidence for a hetero-oligomeric structure in rat brain. J Biol Chem. 1992; 267:501–507. [PubMed: 1309749]

Westrum LE, Blackstad TW. An electron microscopic study of the stratum radiatum of the rat hippocampus (regio superior, CA1) with particular emphasis on synaptology. J Comp Neurol. 1962; 119:281–309. [PubMed: 14000149]

Williams SR, Stuart GJ. Role of dendritic synapse location in the control of action potential output. Trends Neurosci. 2003; 26:147–154. [PubMed: 12591217]

Woolley CS, Wenzel HJ, Schwartzkroin PA. Estradiol increases frequency of multiple synapse boutons in the hippocampal CA1 region of the adult female rat. J Comp Neurol. 1996; 373:108–117. [PubMed: 8876466]

Yankova M, Hart SA, Woolley CS. Estrogen increases synaptic connectivity between single presynaptic inputs and multiple postsynaptic CA1 pyramidal cells: a serial electronmicroscopic study. Proc Natl Acad Sci USA. 2001; 98:3525–3530. [PubMed: 11248111]

Yuste Y, Bonhoeffer T. Morphological changes in dendritic spines associated with long-term synaptic plasticity. Annu Rev Neurosci. 2001; 24:1071–1089. [PubMed: 11520928]

Zhou Q, Homma KJ, Poo MM. Shrinkage of dendritic spines associated with long-term depression of hippocampal synapses. Neuron. 2004; 44:749–757. [PubMed: 15572107]

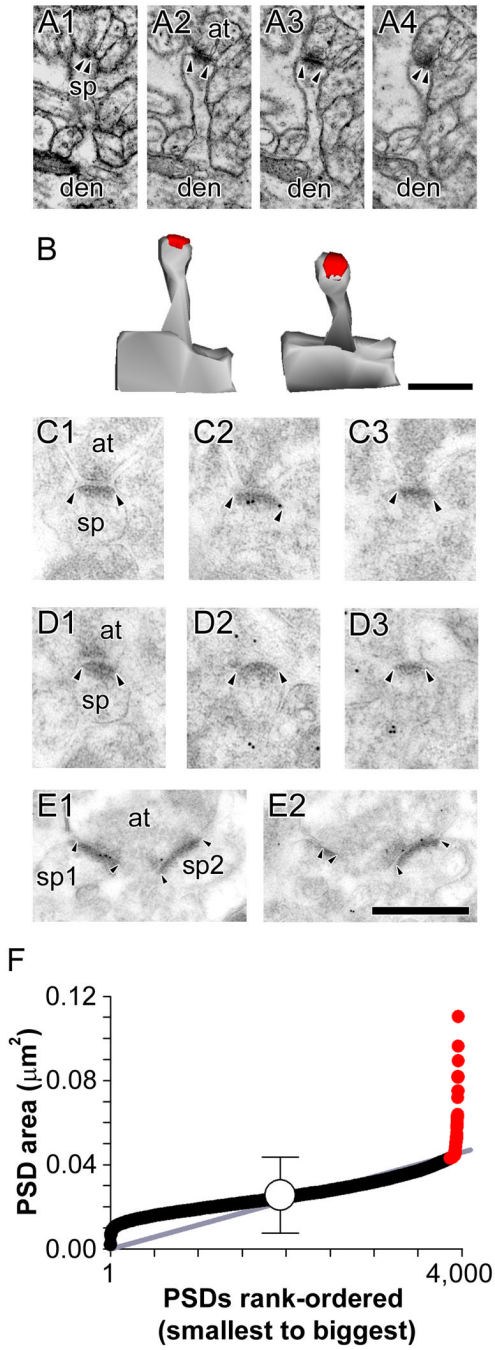

Figure 1. Electron micrographs of "typical" nonperforated synapses

A: Serial sections through a nonperforated (NP) synapse between an axon terminal (at) and a spine (sp) that is seen to connect to its parent dendrite (den). **B:** 3-dimensional reconstructions of the NP synapse and its parent spine in their original orientation (*Left*) and rotated (*Right*) to illustrate the continuous shape of its postsynaptic density (PSD). **C:** Serial sections through a NP synapse (arrowheads) that was immunopositive for AMPA-type receptors (AMPARs). **D:** Serial sections through a NP synapse (arrowheads) that was immunonegative for AMPARs. **E:** Serial sections through two NP synapses (sp1 and sp2; arrowheads) making contact with the same presynaptic axon terminal (at), both of which were immunopositive for NMDA-type receptors. Scale bars = 0.5 μm. **F:** Scatterplot of the

PSD area for all nonperforated synapses in the present study. PSD areas are plotted in rank-order according to their size. Gray line indicates the linear regression that nonperforated synapses follow as they increase in size. Mean PSD size (white circle) is plotted ± 2 standard deviations (S.D.) to illustrate that a subset of NP synapses deviates from the linear trajectory (gray line) at ~ 2 S.D. Such synapses (red circles) were considered atypically large nonperforated (ANP) synapses in the present study.

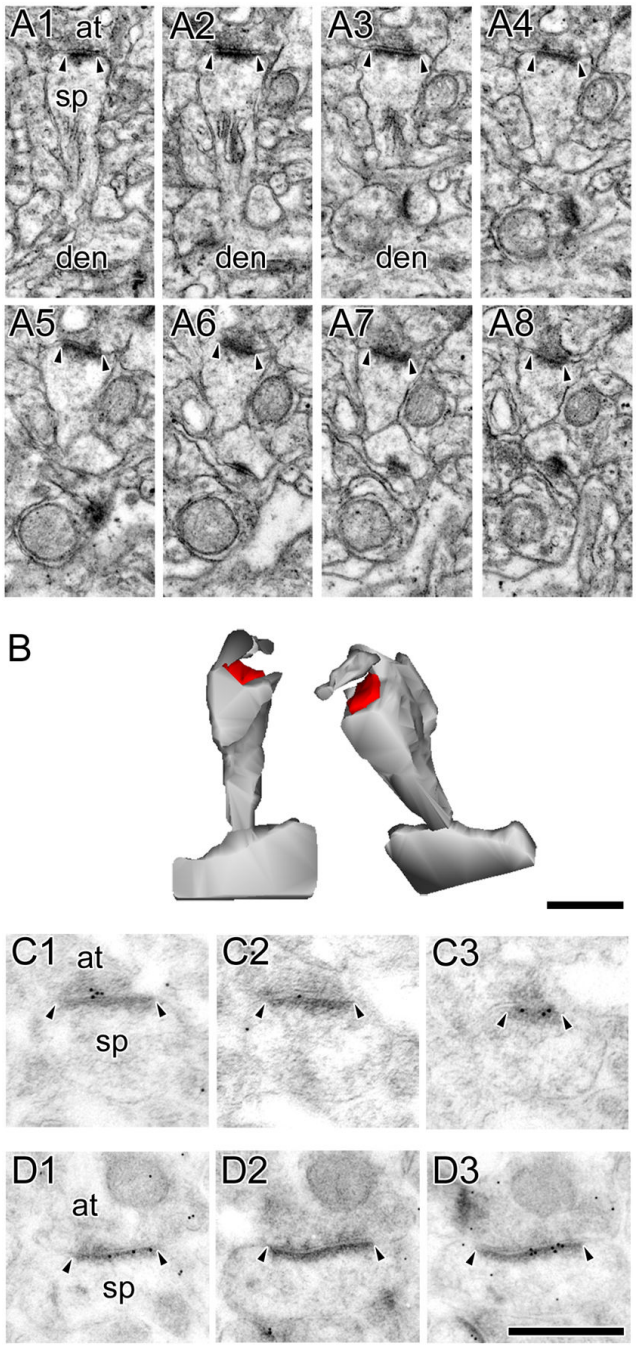

Figure 2. Electron micrographs of atypically large nonperforated synapses

A: Serial sections through an atypically large nonperforated (ANP) synapse (arrowheads) between an axon terminal (at) and a spine (sp), which is seen connecting to its parent dendrite (den). A spine apparatus is observed in the spine head/neck region. **B:** 3-dimensional reconstructions of the ANP synapse and its parent spine in their original orientation (*Left*) and rotated (*Right*) to illustrate the continuous shape and large size of its postsynaptic density (PSD). Note the nonsynaptic spinule emanating from a perisynaptic region of the spine head. **C, D:** Serial sections through ANP synapses between axon terminals (at) and spines (sp), which were always immunopositive for AMPA-type receptors (**C**) and NMDA-type receptors (**D**). Scale bars = 0.5 μm. Though the ANP synapses

showing AMPA-type and NMDA-type are different synapses, all ANP synapses were immunopositive for both. It is likely, then, that each of these synapses, had they been immunostained for both AMPA-type and NMDA-type receptors, would be immunopositive for both. Also note that all but 1 of the immunogold particles in panel C1 are considered synaptic according to our criteria (i.e., on or otherwise within 20 nm of the postsynaptic density, or in the synaptic cleft).

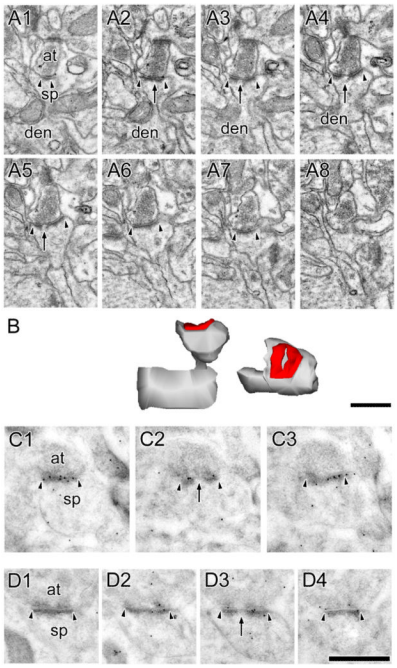

Figure 3. Electron micrographs of perforated synapses with fenestrated postsynaptic densities

A: Serial sections through a perforated synapse with a fenestrated postsynaptic density (PSD; FP synapse) between a spine (sp) protruding from a dendrite (den) and an axon terminal (at). FP synapses are characterized by a hole or fenestration (arrows) in their PSD profile (arrowheads). **B:** 3-dimensional reconstructions of the FP synapse and its parent spine in their original orientation (*Left*) and rotated (*Right*) to illustrate the discontinuity in its PSD. **C, D:** Serial sections through two FP synapses between axon terminals (at) and dendritic spines (sp) showing that FP synapses are highly immunoreactive for AMPA-type receptors (**C**) and NMDA-type receptors (**D**). Scale bars = 0.5 μm.

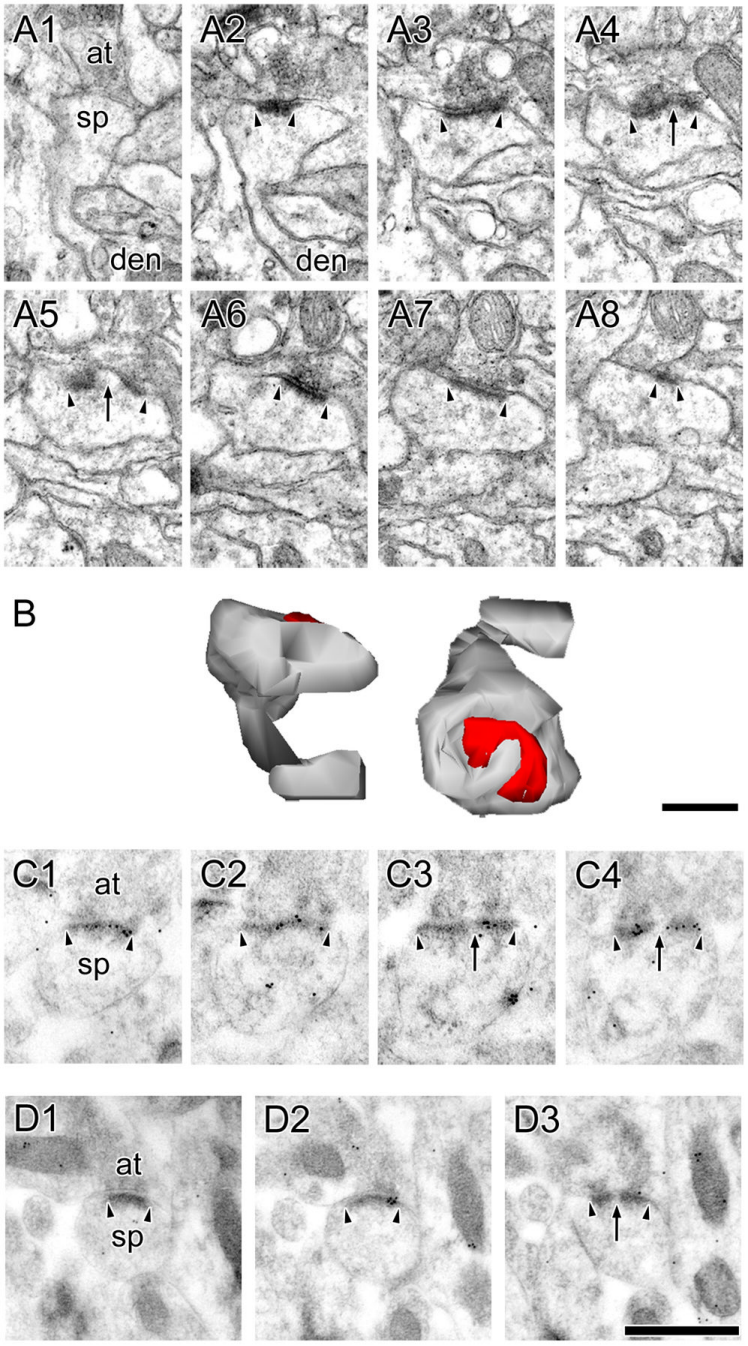

Figure 4. Electron micrographs of perforated synapses with horseshoe-shaped postsynaptic densities

A: Serial sections through a perforated synapse with a horseshoe-shaped postsynaptic density (PSD; HP synapse) between a spine (sp), shown connecting to its parent dendrite (den), and an axon terminal (at). HP synapses are characterized by the appearance of PSD profiles that are initially separated by spine cytoplasm (arrows), but then subsequently can be seen as a single PSD (arrowheads). **B:** 3-dimensional reconstructions of the HP synapse and its parent spine in their original orientation (*Left*) and rotated (*Right*) to illustrate the discontinuity in its PSD. **C, D:** Serial sections through two HP synapses between axon

terminals (at) and dendritic spines (sp) showing that HP synapses are highly immunoreactive for AMPA-type receptors (**C**) and NMDA-type receptors (**D**). Scale bars = 0.5 μm.

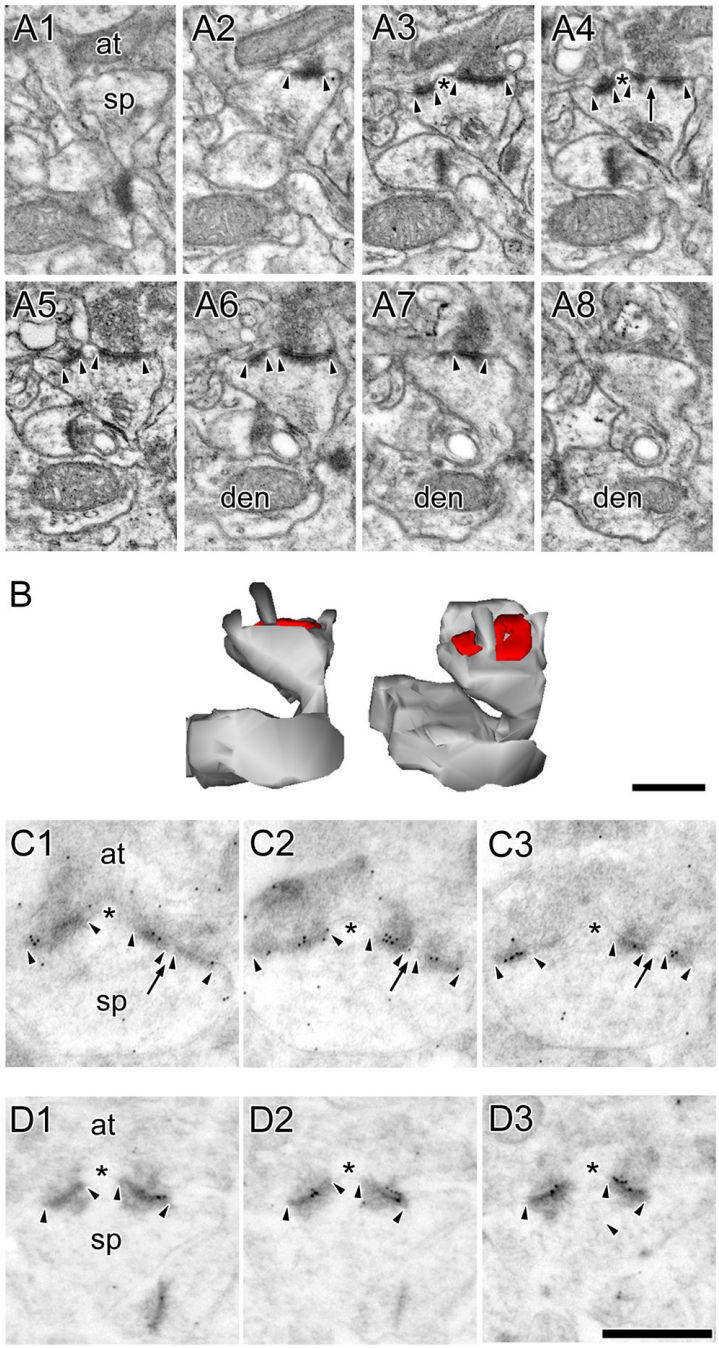

Figure 5. Electron micrographs of perforated synapses with segmented, completely partitioned postsynaptic densities

A: Serial sections through a perforated synapse with a segmented, completed partitioned (SCP) postsynaptic density (PSD; arrowheads) between a spine (sp) on a dendrite (den) and an axon terminal (at). SCP synapses are characterized by multiple PSD profiles (arrowheads), each of which is separated from the other by a complete spine partition (asterisk) that invaginates that presynaptic axon terminal. In the synapse shown, one of the PSD plates is itself discontinuous (arrow). Note the presence of a spine apparatus in the spine head/neck region. **B:** 3-dimensional reconstructions of the SCP synapse and its parent spine in their original orientation (*Left*) and rotated (*Right*) to illustrate that it is composed of

two distinct PSD plates separated by a complete spine partition. **C:** Serial sections through a SCP synapse between an axon terminal (at) and a dendritic spine (sp). The AMPA-type receptor immunoreactivity of SCP synapses is significantly higher than that of other synaptic subtypes in hippocampal region CA1. PSD profiles of the SCP synapse (arrowheads) are separated by a complete spine partition (asterisk) on the one hand, and by a cytoplasmic region of the spine head on the other (arrows). **D:** Serial sections through a SCP synapse between a dendritic spine (sp) and an axon terminal (at), showing the SCP synapses express NMDARs. Note that the PSD plates (arrowheads) are separated from each other by a complete spine partition (asterisk). Note also that each PSD plate of the SCP synapses expresses both AMPARs and NMDARs. Scale bars = 0.5 μm.

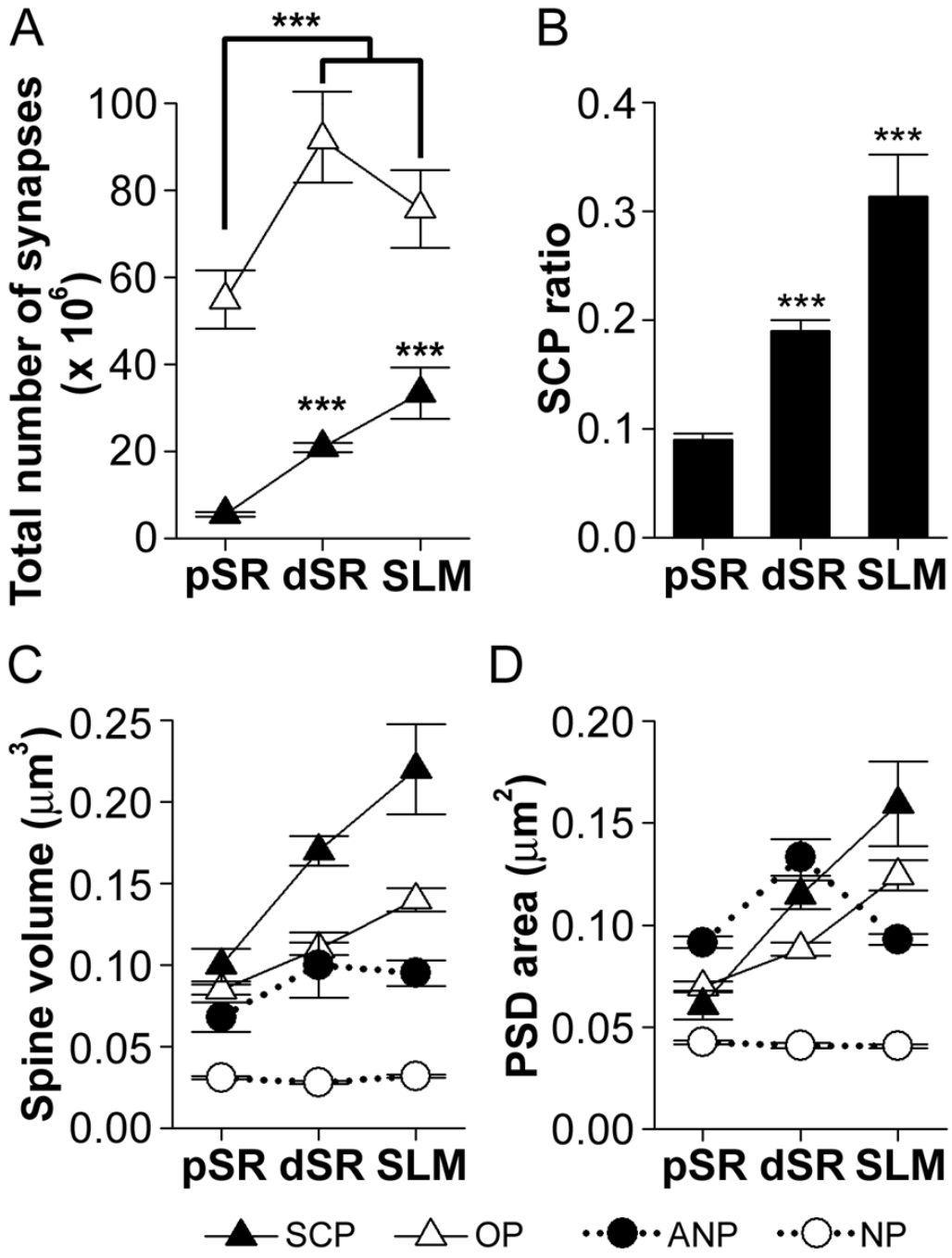

Figure 6. Total number and ratio of segmented, completely partitioned synapses and spine/synapse morphology as a function of dendritic location

A: Total number (± standard error of the mean; S.E.M.) of segmented, completely partitioned (SCP) synapses (black triangles) and other types of perforated (OP) synapses (white triangles) in three regions of the apical dendrite: proximal stratum radiatum (pSR), distal stratum radiatum (dSR), and stratum lacunosum-moleculare (SLM). There were significantly more OP synapses in dSR and SLM as compared to pSR (asterisks). The number of SCP synapses significantly increased with distance from the soma (asterisks). **B:** The ratio (± S.E.M.) of SCP synapses as a function of all perforated synapses increased progressively with distance from the soma (asterisks). **C:** Spine volume for SCP synapses

was highest, whereas that for typical nonperforated (NP; white circles) synapses was lowest in all three dendritic regions. Spine volume for OP and SCP synapses increased with distance from the soma, whereas neither NP nor atypically large nonperforated (ANP; black circles) synapses changed in size as a function of dendritic location. Spine sizes for ANP and OP synapses did not differ significantly from each other. **D:** Postsynaptic density (PSD) area for synapses in pSR, dSR, and SLM. SCP and OP synapses increased in size with distance from the soma, but SCP synapses were bigger in dSR and SLM. ANP synapses were largest in pSR, the same size as SCP synapses in dSR, and intermediate to that of NP and perforated synapses in SLM. NP synapses were the only subtype whose size remained constant in all dendritic regions.

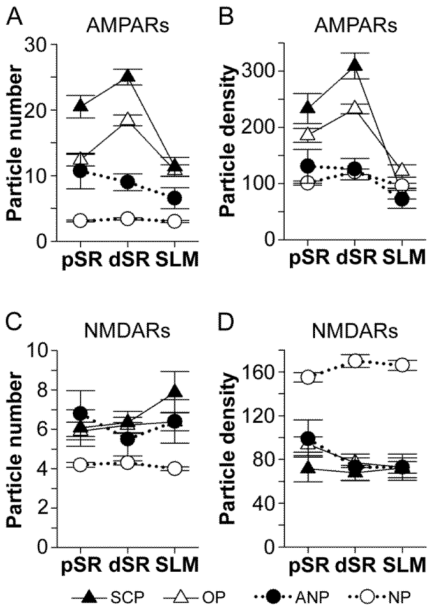

Figure 7. Expression levels of AMPA-type and NMDA-type receptors among the axospinous synaptic subtypes as a function of distance from the soma

A: Immunogold particle number (per synapse) for AMPA-type receptors (AMPARs) for segmented, completely partitioned perforated synapses (SCP; black triangles), other types of perforated synapses (OP; white triangles), as well as nonperforated (NP; white circles) and atypically large nonperforated (ANP; black circles) synapses in three regions of the apical dendrites: proximal stratum radiatum (pSR), distal stratum radiatum (dSR), and stratum lacunosum-moleculare (SLM). SCP synapses had the highest number of particles for AMPARs in pSR and dSR. OP and ANP synapses had the same number of immunogold particles for AMPARs in pSR, but OP synapses had more in dSR. AMPAR immunoexpression did not differ with distance from the soma among NP and ANP synapses, but it increased among SCP and OP synapses between pSR and dSR. In SLM, however, OP and SCP synapses did not differ with respect to their AMPAR immunoreactivity. In dSR and SLM, the level of expression for AMPARs among ANP synapses was intermediate to that of OP and NP synapses. **B:** Density (per μm^2 of postsynaptic density area) of immunogold particles for AMPARs in pSR, dSR, and SLM. Immunogold particle density did not differ between NP and ANP synapses, but OP and SCP synapses had a significantly higher particle density than both nonperforated synaptic subtypes. SCP synapses had the highest particle density in pSR and dSR, but particle density for both OP and SCP synapses increased between pSR and dSR. There were no statistically significant differences among synapses in SLM, except that NP synapses had the lowest particle density. **C:** Immunogold particle number (per synapse) for NMDA-type receptors (NMDARs) in pSR, dSR, and SLM. NMDAR expression did not change with distance from the soma, but NP synapses always had fewer than the other synaptic subtypes. ANP, OP, and SCP synapses did not differ significantly from each other in any dendritic region. **D:** Density (per μm^2 of postsynaptic density area) of immunogold particles for NMDARs was highest among NP synapses. NMDAR immunogold particle density did not change as a function of distance from the soma, nor did it differ among ANP, OP, and SCP synapses.

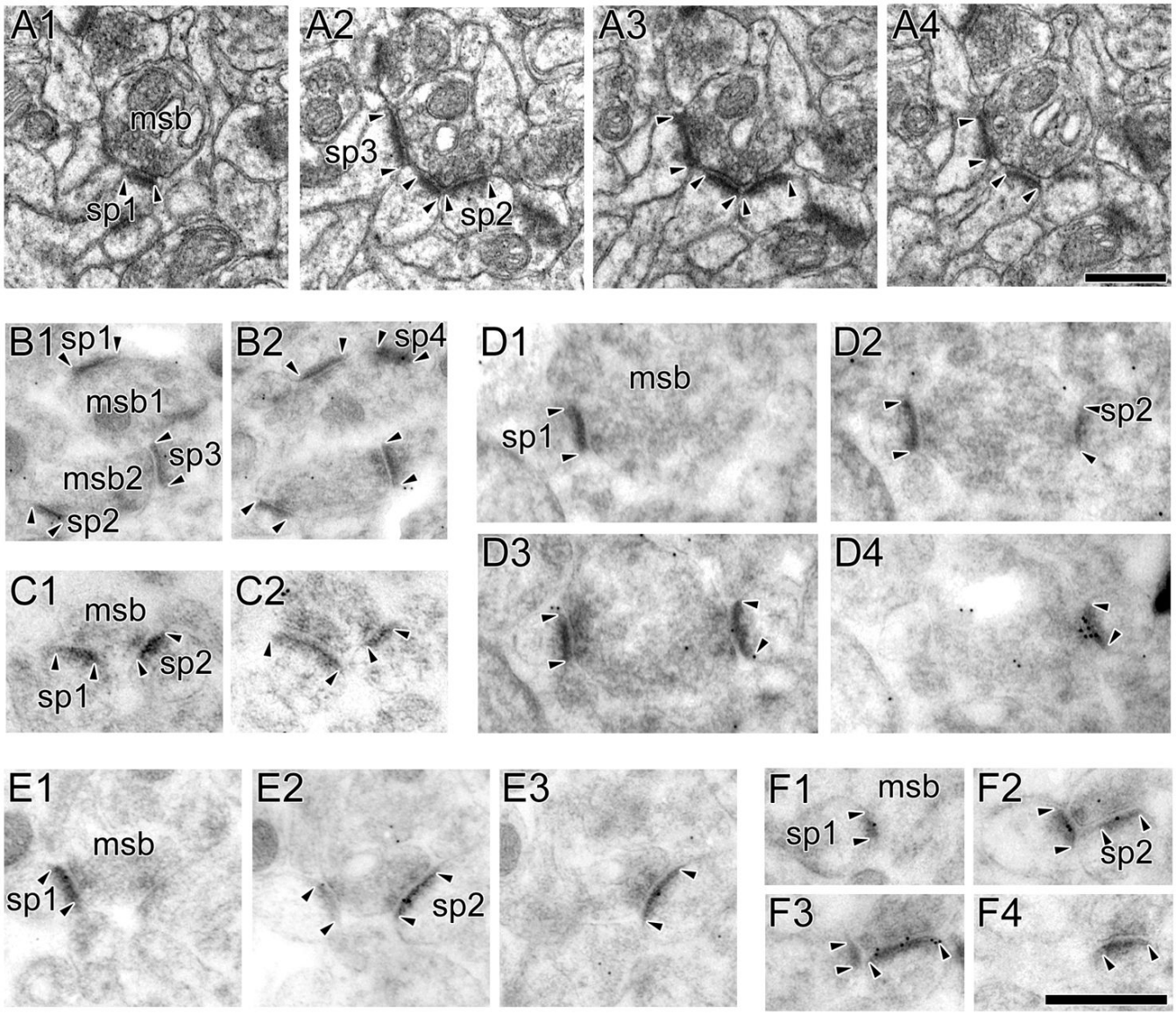

Figure 8. Electron micrographs of multiple synapse boutons involving only nonperforated synapses

A: Serial sections through a multiple synapse bouton (MSB) involving only nonperforated synapses (NP-NP MSB). The axon terminal (msb) synapses with the different spines (sp1, sp2, and sp3), all of which have nonperforated postsynaptic densities (PSD; arrowheads). **B:** Two MSBs (msb1 and msb2) between synapses showing weak AMPA-type receptor (AMPAR) immunoreactivity. One synapse (sp1) does not have any immunogold particles for AMPARs projected onto its PSD, and the others (sp2, sp3, sp4) have only one immunogold particle on their PSD profile. **C:** A NP-NP MSB involving two NP synapses (sp1 and sp2; arrowheads), both of which lack any AMPAR immunoreactivity. **D:** A NP-NP MSB between an axon terminal (msb) and two spines (sp1 and sp2). One synapse has 9 immunogold particles for AMPARs (sp2), whereas the other (sp1) lacks them. **E:** A NP-NP MSB between two spines (sp1 and sp2), both of which are immunoreactive for NMDA-type receptors (NMDARs). **F:** A NP-NP MSB between two spines (sp1 and sp2), which have 3 (sp1) and 8 (sp2) immunogold particles for NMDARs, respectively. Scale bars = 0.5 μm.

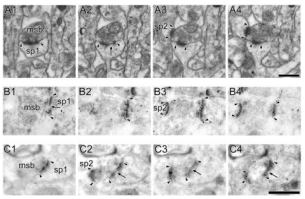

Figure 9. Electron micrographs of multiple synapse boutons involving nonperforated and perforated synapses

A: Serial sections through a multiple synapse bouton (MSB) involving a perforated (sp1) and a nonperforated synapse (sp2; P-NP MSB). The perforated synapse (sp1) is identified by a discontinuity (arrow) in its postsynaptic density (PSD; arrowheads), whereas the PSD of the nonperforated synapse is continuous in all sections (arrowheads). **B:** A P-NP MSB between a perforated (sp1) and a nonperforated (sp2) synapse. The perforated synapse (sp1) has 16 immunogold particles for AMPA-type receptors projected onto its PSD, whereas the nonperforated synapse (sp2) has none. **C:** A P-NP MSB between a perforated (sp1) and a nonperforated (sp2) synapse, both of which are immunoreactive for NMDA-type receptors (NMDARs). The perforated synapse (sp1) shows a discontinuity (arrow) in its PSD profiles (arrowheads), whereas the nonperforated synapse has continuous PSD profiles (arrowheads). The perforated and nonperforated synapses have 7 and 6 immunogold particles for NMDARs projected onto their PSDs, respectively. Scale bars = 0.5 μm.

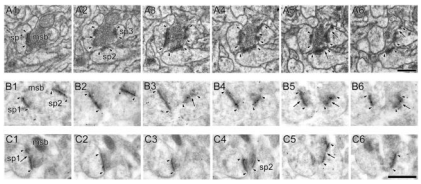

Figure 10. Electron micrographs of multiple synapse boutons involving only perforated synapses

A: Serial sections through a multiple synapse bouton (msb) involving only perforated synapses (sp1, sp2, and sp3; P-P MSB). Each synapse (arrowheads) has at least one discontinuity in its postsynaptic density (PSD) profile (arrows). **B:** A P-P MSB involving two perforated synapses (sp1 and sp2) that are immunoreactive for AMPA-type receptors (AMPARs). One synapse (sp1) has 12 immunogold particles for AMPARs projected onto its PSD, and the other (sp2) has 14. **C:** A P-P MSB involving two perforated synapses (sp1 and sp2) that have 5 (sp1) and 4 (sp2) immunogold particles for NMDA-type receptors. Scale bars = 0.5 μm.

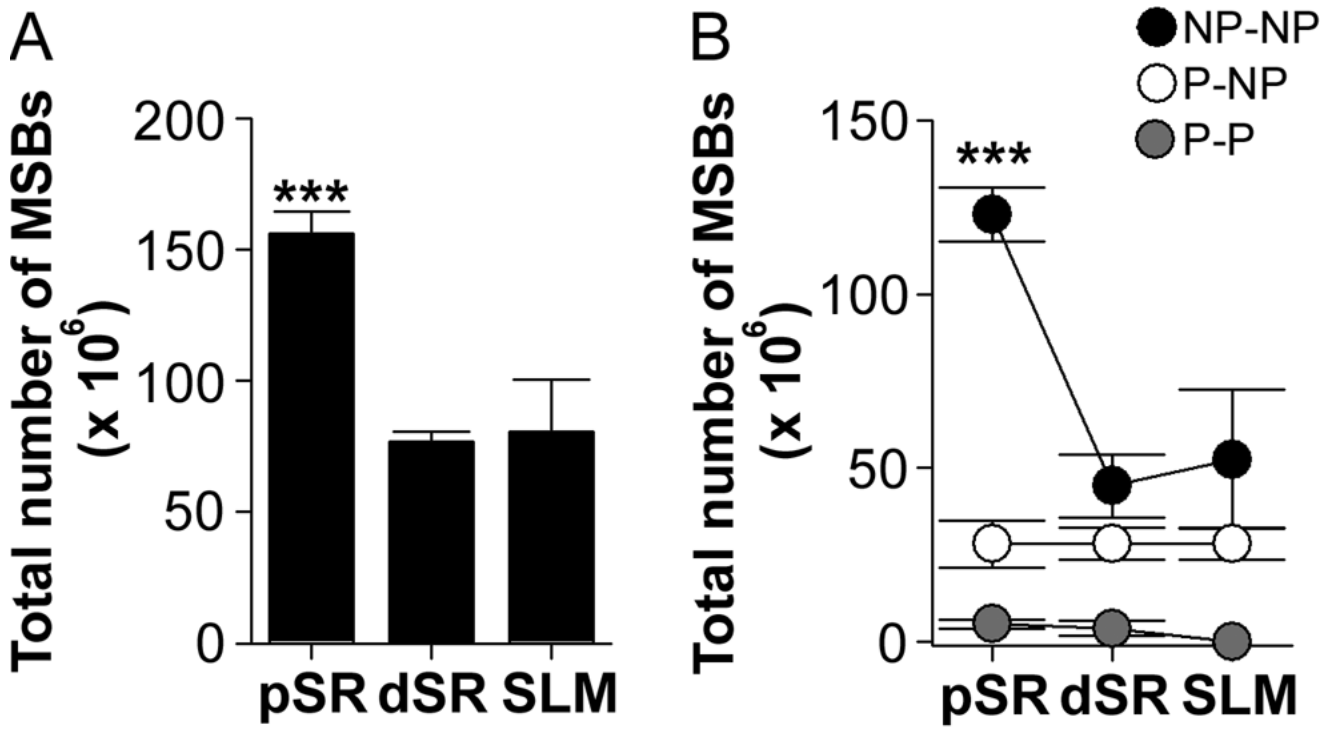

Figure 11. Total number of multiple synapse boutons

A: Proximal stratum radiatum (pSR) had more multiple synapse boutons (MSBs) than both distal stratum radiatum (dSR) and stratum lacunosum-moleculare (SLM; asterisks). **B:** pSR had more MSBs involving exclusively nonperforated synapses (NP-NP MSB; black circles) than dSR or SLM (asterisks). The total number of MSBs involving either perforated and nonperforated synapses (P-NP MSB; white circles) or exclusively perforated synapses (P-P MSB; gray circles) did not differ among the three apical dendritic regions.

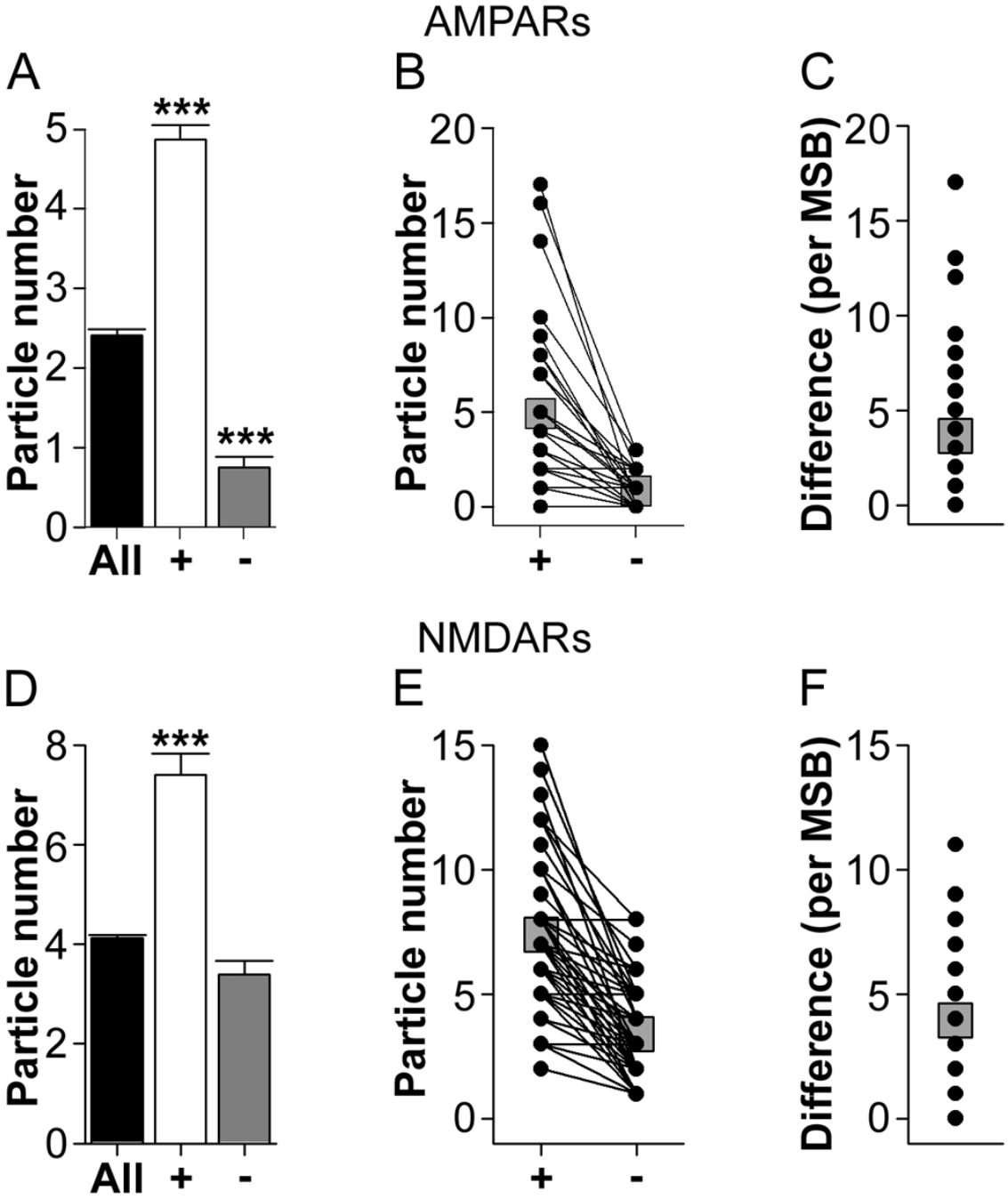

Figure 12. Expression of AMPA-type and NMDA-type receptors in synapses of multiple synapse boutons that involve only nonperforated synapses

A: Average immunogold particle number for AMPA-type receptors (AMPARs) for all nonperforated (NP) synapses in the present study (black bar), the synapse with the higher number of immunogold particles in each nonperforated synapse-only multiple synapse bouton (NP-NP MSB; plus sign), and the synapse with the lower number of immunogold particles in each NP-NP MSB (minus sign). Asterisks indicate that NP-NP MSBs, on average, involved a nonperforated synapse with an abnormally high level of AMPAR expression and one with a significantly lower level of AMPAR expression compared to the overall population of NP synapses. **B:** Immunogold particles for AMPARs for each synapse

involved in each NP-NP MSB, plotted according to which synapse had a higher (plus sign) or lower (minus sign) number. **C:** The difference in the immunogold particle number for AMPARs between the synapses of each NP-NP MSB. **D:** Average immunogold particle number for NMDA-type receptors (NMDARs) for all nonperforated (NP) synapses in the present study (black bar), the synapse with the higher number of immunogold particles in each NP-NP MSB (plus sign), and the synapse with the lower number of immunogold particles in each NP-NP MSB (minus sign). Asterisks indicate that NP-NP MSBs, on average, involved a nonperforated synapse with an abnormally high level of NMDAR expression and one with an expression level typical of the overall population. **E:** Immunogold particles for NMDARs for each synapse involved in each NP-NP MSB, plotted according to which synapse had a higher (plus sign) or lower (minus sign) number. **F:** The difference in the immunogold particle number for NMDARs between the synapses of each NP-NP MSB. Means are plotted in **B**, **C**, **E**, and **F** as gray squares.

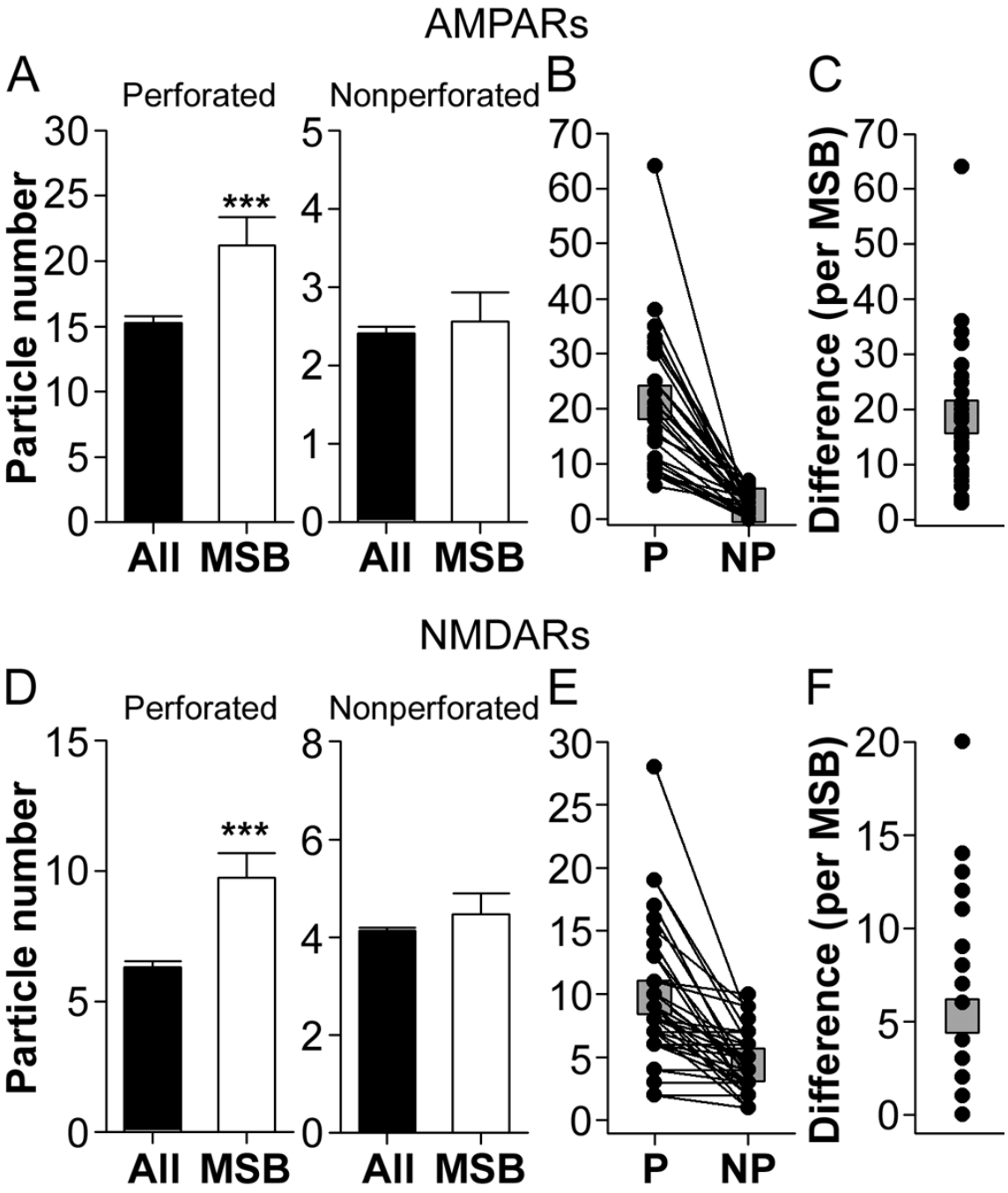

Figure 13. Expression of AMPA-type and NMDA-type receptors in synapses of multiple synapse boutons that involve a mix of nonperforated and perforated synapses

A: *Left panel* Average immunogold particle number for AMPA-type receptors (AMPARs) for all perforated synapses in the present study (black bar), and for the perforated synapses of each perforatednonperforated synapse multiple synapse bouton (P-NP MSB; white bar). The asterisk indicates that perforated synapses involved in P-NP MSBs have a higher level of AMPAR expression than would be expected from the overall population of perforated synapses. *Right panel* Average immunogold particle number for AMPARs for all nonperforated (NP) synapses in the present study (black bar), and for the NP synapses of each P-NP MSB (white bar). **B:** Immunogold particles for AMPARs for each synapse

involved in each P-NP MSB, plotted according to whether its PSD was perforated (P) or nonperforated (NP). **C:** The difference in the immunogold particle number for AMPARs between the synapses of each P-NP MSB. **D:** *Left panel* Average immunogold particle number for NMDA-type receptors (NMDARs) for all perforated synapses in the present study (black bar), and for the perforated synapses of each P-NP MSB (white bar). The asterisk indicates that perforated synapses involved in P-NP MSBs have a higher level of NMDAR expression than would be expected from the overall population of perforated synapses. *Right panel* Average immunogold particle number for NMDARs for all NP synapses in the present study (black bar), and for the NP synapses of each P-NP MSB (white bar). **E:** Immunogold particles for NMDARs for each synapse involved in each P-NP MSB, plotted according to whether its PSD was perforated (P) or nonperforated (NP). **F:** The difference in the immunogold particle number for NMDARs between the synapses of each P-NP MSB. Means are plotted in **B**, **C**, **E**, and **F**as gray squares.

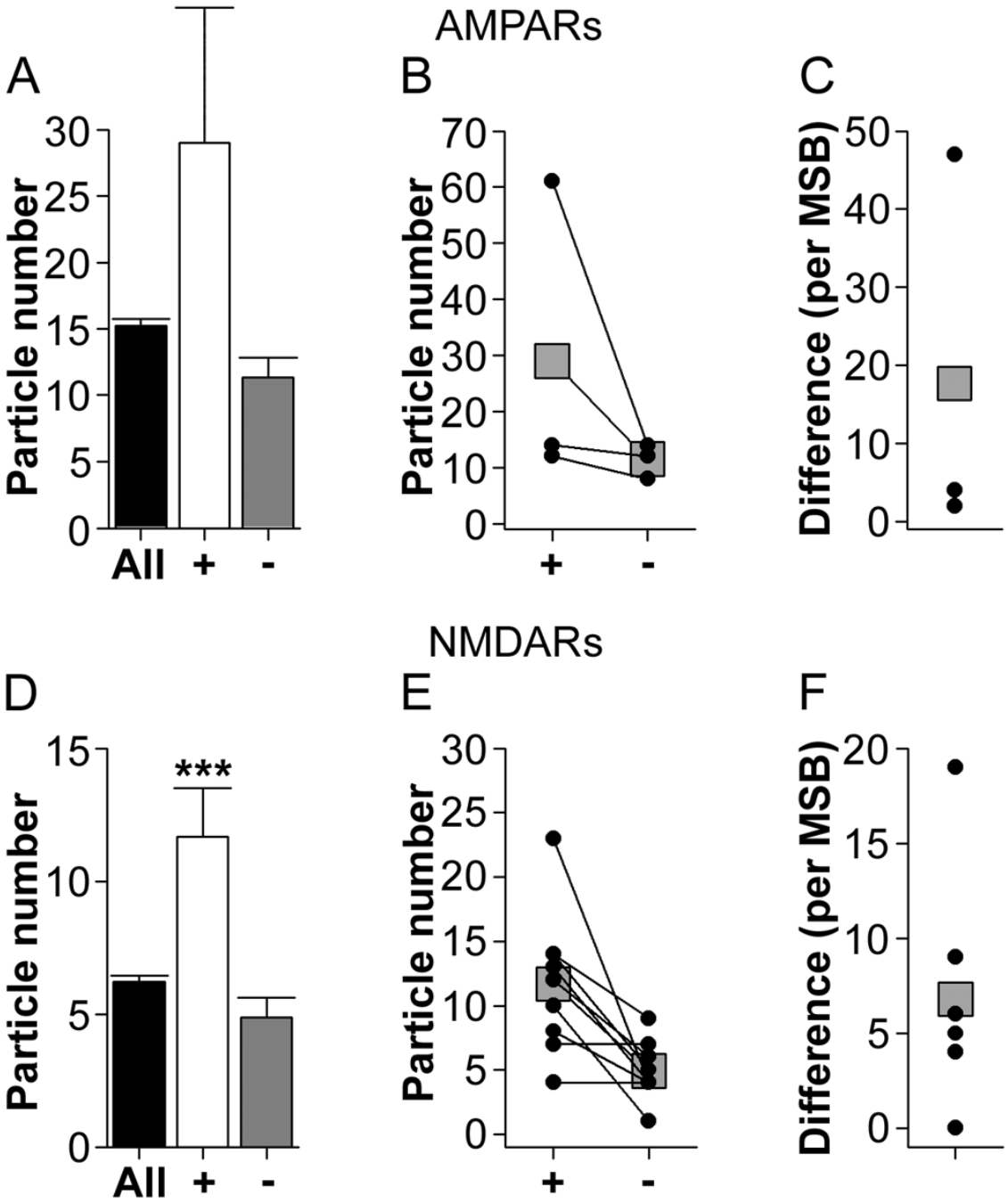

Figure 14. Expression of AMPA-type and NMDA-type receptors in synapses of multiple synapse boutons that involve only perforated synapses

A: Average immunogold particle number for AMPA-type receptors (AMPARs) for all perforated synapses in the present study (black bar), the synapse with the higher number of immunogold particles in each perforated synapse-only multiple synapse bouton (P-P MSB; plus sign), and the synapse with the lower number of immunogold particles in each P-P MSB (minus sign). **B:** Immunogold particles for AMPARs for each synapse involved in each P-P MSB, plotted according to which synapse had a higher (plus sign) or lower (minus sign) number. **C:** The difference in the immunogold particle number for AMPARs between the synapses of each P-P MSB. **D:** Average immunogold particle number for NMDA-type

receptors (NMDARs) for all perforated synapses in the present study (black bar), the synapse with the higher number of immunogold particles in each P-P MSB (plus sign), and the synapse with the lower number of immunogold particles in each P-P MSB (minus sign). **E:** Immunogold particles for NMDARs for each synapse involved in each P-P MSB, plotted according to which synapse had a higher (plus sign) or lower (minus sign) number. **F:** The difference in the immunogold particle number for NMDARs between the synapses of each P-P MSB. Means are plotted in **B**, **C**, **E**, and **F** as gray squares.

Table 1

Structure and receptor expression of synaptic subtypes in proximal stratum radiatum

	NP		ANP		OP		SCP	
	n	**Mean (Range)**	**n**	**Mean (Range)**	**n**	**Mean (Range)**	**n**	**Mean (Range)**
Conventional								
Structure								
Spine volume (μm^3)	207	0.029 (0.007-0.128)	11	0.0.068 (0.051-0.112)	83	0.085 (0.026-.212)	10	0.103 (0.068-0.142)
PSD area (μm^2)	207	0.042 (0.018-0.074)	11	0.091 (0.084-0.115)	83	0.070 (0.022-.155)	10	0.073 (0.026-0.183)
Spine neck length (nm)	164	202 (58-880)	10	298 (133-516)	77	309 (78-880)	10	290 (82-574)
Spine neck width (nm)	207	146 (45-988)	11	121 (42-235)	83	117 (39-707)	10	113 (82-142)
Parent dendrite (nm)	203	603 (237-1858)	9	560 (328-820)	73	507 (257-1728)	8	497 (347-848)
Spine apparatus	0/207		3/11		15/83		3/10	
Postembedding immunogold								
AMPAR immunoreactivity								
Particle number	500	3.1 (1-28)	17	10.7 (1-39)	93	12.4 (1-40)	12	20.6 (14-37)
Particle density (per μm^2 PSD area)	500	101 (18-615)	17	131 (7-587)	93	187 (18-571)	12	233 (140-472)
NMDAR immunoreactivity								
Particle number	606	4.2 (1-19)	13	6.8 (1-13)	78	6.0 (1-21)	15	6.1 (1-13)
Particle density (per μm^2 PSD area)	606	155 (16-634)	13	99 (14-195)	78	94 (12-322)	15	73 (15-182)

Table 2

Structure and receptor expression of synaptic subtypes in distal stratum radiatum

	NP		ANP		OP		SCP	
	n	**Mean (Range)**	**n**	**Mean (Range)**	**n**	**Mean (Range)**	**n**	**Mean (Range)**
Conventional								
Structure								
Spine volume (μm^3)	199	0.028 (0.006-0.147)	10	0.105 (0.035-0.22)	119	0.112 (0.02-0.24)	42	0.174 (0.077-0.322)
PSD area (μm^2)	199	0.041 (0.014-0.094)	10	0.133 (0.103-0.199)	119	0.088 (0.027-.224)	42	0.115 (0.031-0.211)
Spine neck length (nm)	152	232 (83-720)	6	361 (112-817)	119	329 (78-880)	34	337 (87-800)
Spine neck width (nm)	198	134 (37-558)	8	160 (83-325)	119	144 (40-577)	42	143 (27-361)
Parent dendrite (nm)	177	653 (243-1693)	7	607 (380-1580)	98	561 (233-1526)	35	581 (282-1449)
Spine apparatus	0/199		7/10		26/119		34/42	
Postembedding immunogold								
AMPAR immunoreactivity								
Particle number	485	3.4 (1-21)	29	8.9 (1-28)	161	18.4 (4-44)	29	25 (8-67)
Particle density (per μm^2 PSD area)	485	121 (19-816)	29	126 (15-456)	161	232 (42-542)	29	309 (118-613)
NMDAR immunoreactivity								
Particle number	743	4.3 (1-17)	16	5.5 (2-13)	114	6.2 (1-19)	23	6.3 (3-13)
Particle density (per μm^2 PSD area)	743	166 (20-853)	16	74 (25-180)	114	77 (17-276)	23	68 (22-139)

Table 3

Structure and receptor expression of synaptic subtypes in stratum lacunosum-moleculare

	NP		ANP		OP		SCP	
	n	**Mean (Range)**	**n**	**Mean (Range)**	**n**	**Mean (Range)**	**n**	**Mean (Range)**
Conventional								
Structure								
Spine volume (μm^3)	110	0.031 (0.006-0.124)	9	0.095 (0.070-0.142)	58	0.143 (0.037-0.326)	49	0.228 (0.065-0.515)
PSD area (μm^2)	110	0.041 (0.018-0.081)	9	0.092 (0.082-0.101)	58	0.124 (0.039-0.334)	49	0.160 (0.062-0.421)
Spine neck length (nm)	74	346 (113-920)	8	368 (141-617)	55	322 (89-781)	43	387 (52-1242)
Spine neck width (nm)	98	149 (43-407)	9	137 (52-322)	58	170 (47-421)	49	200 (66-518)
Parent dendrite (nm)	101	336 (137-1058)	9	360 (155-720)	47	328 (198-580)	38	324 (128-597)
Spine apparatus	0/110		2/9		31/58		34/49	
Postembedding immunogold								
AMPAR immunoreactivity								
Particle number	262	3.0 (1-16)	13	6.5 (1-22)	97	10.8 (1-43)	39	11.3 (1-50)
Particle density (per μm^2 PSD area)	262	96 (15-593)	13	72 (9-212)	97	122 (10-480)	39	82 (16-298)
NMDAR immunoreactivity								
Particle number	633	4.2 (1-19)	14	6.4 (1-13)	101	6.4 (1-24)	25	7.98 (1-26)
Particle density (per μm^2 PSD area)	633	165 (16-609)	14	73 (12-154)	101	73 (6-273)	25	72 (8-184)

Table 4

AMPAR and NMDAR expression of synapses involved in multiple synapse boutons (MSBs) throughout the apical dendrites of CA1

Proximal stratum radiatum				**Distal stratum radiatum**				**Stratum lacunosum-moleculare**			
	Particle number		**n**		**Particle number**		**n**		**Particle number**		**n**
MSB Subtype	**(Average ± S.E.M)**			***MSB Subtype***	**(Average ± S.E.M)**			***MSB Subtype***	**(Average ± S.E.M)**		
NP-NP				**NP-NP**				**NP-NP**			
AMPAR	Higher: 5.1	(±1.02)	16	AMPAR	Higher: 4.4	(±1.18)	18	AMPAR	Higher: 2.9	(±0.64)	10
	Lower: 1.2	(±0.29)			Lower: 0.4	(±0.18)			Lower: 0.9	(±0.28)	
NMDAR	Higher: 6.5	(±0.64)	15	NMDAR	Higher: 7.9	(±0.80)	15	NMDAR	Higher: 7.7	(±0.71)	19
	Lower: 3.5	(±0.42)			Lower: 4.1	(±0.55)			Lower: 3.0	(±0.43)	
P-NP				**P-NP**				**P-NP**			
AMPAR	Higher: 19.8	(±2.35)	9	AMPAR	Higher: 26.1	(±4.79)	14	AMPAR	Higher: 15.0	(±3.80)	9
	Lower: 2.8	(±0.91)			Lower: 2.8	(±0.54)			Lower: 2.11	(±0.65)	
NMDAR	Higher: 10.0	(±1.69)	9	NMDAR	Higher: 7.6	(±1.46)	11	NMDAR	Higher: 11.2	(±1.62)	14
	Lower: 4.8	(±0.64)			Lower: 4.4	(±0.80)			Lower: 4.9	(±0.78)	
P-P				**P-P**				**P-P**			
AMPAR	Higher: 12	(±0)	1	AMPAR	Higher: 61	(±0)	1	AMPAR	Higher: 14	(±0)	1
	Lower: 8	(±0)			Lower: 14	(±0)			Lower: 12	(±0)	
NMDAR	Higher: 6.0	(±2.0)	2	NMDAR	Higher: 16.0	(±3.51)	3	NMDAR	Higher: 11.3	(±1.71)	4
	Lower: 4.0	(±0)			Lower: 4.7	(±0.67)			Lower: 5.5	(±1.71)	